NAVAL POSTGRADUATE SCHOOL
Monterey, California

THESIS

THE BOTTOM BOUNDARY LAYER UNDER SHOALING INNER SHELF SOLITONS

by

Kristi Mae Tjoa

June 2003

Thesis Advisor:	Timothy P. Stanton
Second Reader:	Edward B. Thornton

THIS PAGE INTENTIONALLY LEFT BLANK

REPORT DOCUMENTATION PAGE			Form Approved OMB No. 0704-0188
Public reporting burden for this collection of information is estimated to average 1 hour per response, including the time for reviewing instruction, searching existing data sources, gathering and maintaining the data needed, and completing and reviewing the collection of information. Send comments regarding this burden estimate or any other aspect of this collection of information, including suggestions for reducing this burden, to Washington headquarters Services, Directorate for Information Operations and Reports, 1215 Jefferson Davis Highway, Suite 1204, Arlington, VA 22202-4302, and to the Office of Management and Budget, Paperwork Reduction Project (0704-0188) Washington DC 20503.			
1. AGENCY USE ONLY *(Leave blank)*	**2. REPORT DATE** June 2003	**3. REPORT TYPE AND DATES COVERED** Master's Thesis	
4. TITLE AND SUBTITLE: The Bottom Boundary Layer Under Shoaling Inner Shelf Solitons			**5. FUNDING NUMBERS**
6. AUTHOR(S) Tjoa, Kristi M.			
7. PERFORMING ORGANIZATION NAME(S) AND ADDRESS(ES) Naval Postgraduate School Monterey, CA 93943-5000			**8. PERFORMING ORGANIZATION REPORT NUMBER**
9. SPONSORING /MONITORING AGENCY NAME(S) AND ADDRESS(ES) N/A			**10. SPONSORING/MONITORING AGENCY REPORT NUMBER**
11. SUPPLEMENTARY NOTES The views expressed in this thesis are those of the author and do not reflect the official policy or position of the Department of Defense or the U.S. Government.			
12a. DISTRIBUTION / AVAILABILITY STATEMENT Approved for public release; distribution is unlimited			**12b. DISTRIBUTION CODE**

13. ABSTRACT

The effects of shoaling inner shelf solitons on the bottom boundary layer have been observed and analyzed over a two month summer period at the Monterey Inner Shelf Observatory in Monterey, CA, during 2002. Utilizing CTD data to characterize the temperature field of the water column, Acoustic Doppler Current Profiler (ADCP) data to measure the velocity structure from 3m height above the bed (HAB) to the near surface, and Bistatic Doppler Velocity Sediment Profiler (BDVSP) data to measure the velocity structure and sediment concentration from a range of 60cm to 1cm HAB, solitary internal waves and internal tidal bores were regularly observed at the observation site. These events were characterized by their large isotherm displacements and the sudden change from near surface to near bed stratification as the internal tidal bores passed the observation site. Cross-shore timeseries revealed that the strongest events pushed water onshore near the surface and offshore near the bed, indicating a baroclinic water column during their passage. To analyze their effects on the bottom boundary layer, 3m HAB ADCP and BCDV velocities were compared with backscatter data and surface gravity wave energy at 3m HAB to determine their relative contribution to bed stress and resulting sediment suspension. As the strong internal waves passed, a logarithmic layer formed indicating that shear stress above the bed was occurring. This allowed the friction velocity within the log layer to be estimated. Combining this term with the stress contribution due to the wave energy, the total stress on the bed was then estimated. From this it was determined that typically moderate surface gravity wave forcing at the bed suspended sediment, while solitary internal waves and internal tidal bores continued to transport suspended sediment offshore near the bed.

14. SUBJECT TERMS Oceanography, Nearshore, Waves, Currents, Tides, Internal Tidal Bores, Solitons, Sediment Suspension, Sediment Transport			**15. NUMBER OF PAGES** 99
			16. PRICE CODE
17. SECURITY CLASSIFICATION OF REPORT Unclassified	**18. SECURITY CLASSIFICATION OF THIS PAGE** Unclassified	**19. SECURITY CLASSIFICATION OF ABSTRACT** Unclassified	**20. LIMITATION OF ABSTRACT** UL

NSN 7540-01-280-5500 Standard Form 298 (Rev. 2-89)
Prescribed by ANSI Std. 239-18

THIS PAGE INTENTIONALLY LEFT BLANK

Approved for public release; distribution is unlimited.

THE BOTTOM BOUNDARY LAYER UNDER SHOALING INNER SHELF SOLITONS

Kristi Mae Tjoa
Ensign, United States Navy
B.S., United States Naval Academy, 2002

Submitted in partial fulfillment of the
requirements for the degree of

MASTER OF SCIENCE IN PHYSICAL OCEANOGRAPHY

from the

NAVAL POSTGRADUATE SCHOOL
June 2003

Author: Kristi Mae Tjoa

Approved by: Timothy P. Stanton
Thesis Advisor

Edward B. Thornton
Second Reader

Mary L. Batten
Chairman, Department of Oceanography

THIS PAGE INTENTIONALLY LEFT BLANK

ABSTRACT

The effects of shoaling inner shelf solitons on the bottom boundary layer have been observed and analyzed over a two month summer period at the Monterey Inner Shelf Observatory in Monterey, CA, during 2002. Utilizing CTD data to characterize the temperature field of the water column, Acoustic Doppler Current Profiler (ADCP) data to measure the velocity structure from 3m height above the bed (HAB) to the near surface, and Bistatic Doppler Velocity Sediment Profiler (BDVSP) data to measure the velocity structure and sediment concentration from a range of 60cm to 1cm HAB, solitary internal waves and internal tidal bores were regularly observed at the observation site. These events were characterized by their large isotherm displacements and the sudden change from near surface to near bed stratification as the internal tidal bores passed the observation site. Cross-shore timeseries revealed that the strongest events pushed water onshore near the surface and offshore near the bed, indicating a baroclinic water column during their passage. To analyze their effects on the bottom boundary layer, 3m HAB ADCP and BCDV velocities were compared with backscatter data and surface gravity wave energy at 3m HAB to determine their relative contribution to bed stress and resulting sediment suspension. As the strong internal waves passed, a logarithmic layer formed indicating that shear stress above the bed was occurring. This allowed the friction velocity within the log layer to be estimated. Combining this term with the stress contribution due to the wave energy, the total stress on the bed was then estimated. From this it was determined that typically moderate surface gravity wave forcing at the bed suspended sediment, while solitary internal waves and internal tidal bores continued to transport suspended sediment offshore near the bed.

THIS PAGE INTENTIONALLY LEFT BLANK

TABLE OF CONTENTS

LIST OF FIGURES

THIS PAGE INTENTIONALLY LEFT BLANK

ACKNOWLEDGMENTS

I would like to thank my advisor, Professor Tim Stanton, for sparking my interest and curiosity in the field of near-shore oceanography and for allowing me to work with an amazing data set. I am grateful to him for his patience, guidance, and confidence in my abilities to learn and understand the concepts as well as MATLAB. He provided me with the necessary motivation to challenge myself by working independently to solve problems.

I would also like to thank the Office of Naval Research for sponsoring the Shoaling Waves Experiment (SHOWEX) of which MISO is a part of, as well as the ocean turbulence group at NPS for their dedication to the development and maintenance of MISO and its instruments.

Most of all, thank you to my parents who have supported and encouraged me through all my academic endeavors. And, to the 2003 IGEP oceanographers, (ENS Colleen O'Malley, ENS Tim Ray, ENS Rob Holt, and ENS Mathias Roth) for their support and commitment to each other and to the program. Last, but not least, to my friend Seth Johnson for his unwavering support through all the tough times and for always believing in me.

THIS PAGE INTENTIONALLY LEFT BLANK

I. INTRODUCTION

Surface disturbances caused by strong, nonlinear, near-surface internal waves are commonly seen over the continental shelf as bands of slick and rough water propagating shoreward (Kropfli et al 1998). These internal waves, or solitons, evolve on the leading edge of an internal tidal bore that has steepened due to dispersion effects. As these solitons propagate shoreward and begin to shoal, their form changes, and they start to affect the bottom boundary layer above the ocean bed. From their first observation in 1834 by John Scott Russel as a surface disturbance propagating down a canal, few studies have been conducted on their effect on the bottom boundary layer. Past studies have primarily been focused offshore and on their effects on the current and temperature fields as well as their dynamics. Studies conducted by Baines (1972) in the Mid-Atlantic Ridge, Apel (1985) in the Sulu Sea, and Holloway (1987) off northwest Australia were mainly focused on internal tide generation over a shelf break and on characterizing the resulting solitons. More recent studies conducted by Liu (1988) and Chapman et al (1997) in the New York Bight and Stanton and Ostrovsky (1998) off northern Oregon began to focus on solitons as they propagated away from their generation site. Still, little has been discussed on soliton effects further inshore on the shelf and their effects on the bottom boundary layer due to shoaling. Liu (1988) briefly touched on the shoaling parameter as it relates to soliton growth and decay. The purpose of the inner shelf soliton experiment conducted in Monterey Bay during the summer of 2002 was to closely examine soliton and internal tidal bore effects on the bottom boundary layer due to shoaling at an inner shelf site only 600m from the surf zone.

Certain environmental conditions are necessary to allow an internal tide and solitons to develop in coastal regions. Strong, shallow stratification in the water column, which frequently approximates a two-layer system, provides the background for these waves to form (Stanton and Ostrovsky 1998). A significant cross-shelf barotropic tidal current provides the necessary forcing in order to generate an internal tide. This internal tide propagates shoreward as an internal tidal bore, and the baroclinic structure of the bore causes water near the surface to be pushed onshore and water nearer the bed to be

pulled offshore. As the leading edge of the tidal bore steepens it begins to degenerate into solitons due to the dispersive properties of internal waves. These solitons have the same baroclinic structure as the tidal bore, but with much shorter wavelengths, and cause currents to flow in the same pattern. The main objective in the bottom boundary analysis is to prove that the strong push and pull of water associated with tidal bores and solitons are felt near the surface and all the way down the water column to the bed. From this it can be shown if stresses generated by offshore movement of water near the bed act together with near bed forcing from surface gravity waves to disrupt the bed and cause sediment to be suspended and thus, produce a significant net transport.

The location and complexity of the shelf break plays a significant role in the propagation of internal bores. As in previous studies conducted, the location of the shelf break was approximately parallel to the coast causing Stanton (1998), Liu (1988), Chapman (1997) and others to conclude that tidal bore and soliton propagation are largely cross-shelf, with currents moving on and offshore. However, due to the complexity of the shelf break and canyon within Monterey Bay, it is likely that internal tidal bores might have significant alongshore (AS) components. It is hypothesized that the morphology of the Monterey Canyon to the north of our observation site has caused this change in direction and has funneled the internal tide up through the canyon axis and refracted it along its steep walls.

The Monterey Inner Shelf Observatory (MISO) was designed and implemented by Stanton (1999) to provide a long-term observation capability to study the evolution of a sandy bed at an inner shelf site. The objective of this paper is to analyze the effects of tidal bores and solitons on the bottom boundary layer by measuring stress components, sediment suspension profiles, net transport, and to characterize the solitary internal wave and internal tidal bore summer climatology at the site.

A. BACKGROUND

A regional study on the offshore and onshore oceanographic and climatological conditions of Monterey Bay was conducted for the year prior to bottom boundary layer observations. The main objective of this regional study was to look at seasonal scale

changes in the oceanographic structure that determine the presence or absence of internal tidal bores within the bay.

1. Monterey Bay

Monterey Bay is located along the central California coast between 121°W–123°W longitude and 35°N–37°N latitude (Figure 1). The bathymetry offshore of central California is complex, with canyons and ridges dominating the underwater topography as seen in Figure 1. MISO is located in the southern end of Monterey Bay on the inner shelf. North of the MISO site and at the center of the bay is the Monterey Canyon, which reaches depths of up to 4000m. The Monterey Canyon is a classic example of a submarine canyon. Several studies have been conducted to determine the effects on the internal tide within the canyon (Petruncio et al 1997). As the canyon winds its way into Monterey Bay, it cuts into the shelf break with its steep walls and complex bathymetry. The southern edge of the Monterey Canyon wall provides a steep shelf break area north of the MISO site, with depths jumping from 1000m to 100m over a short

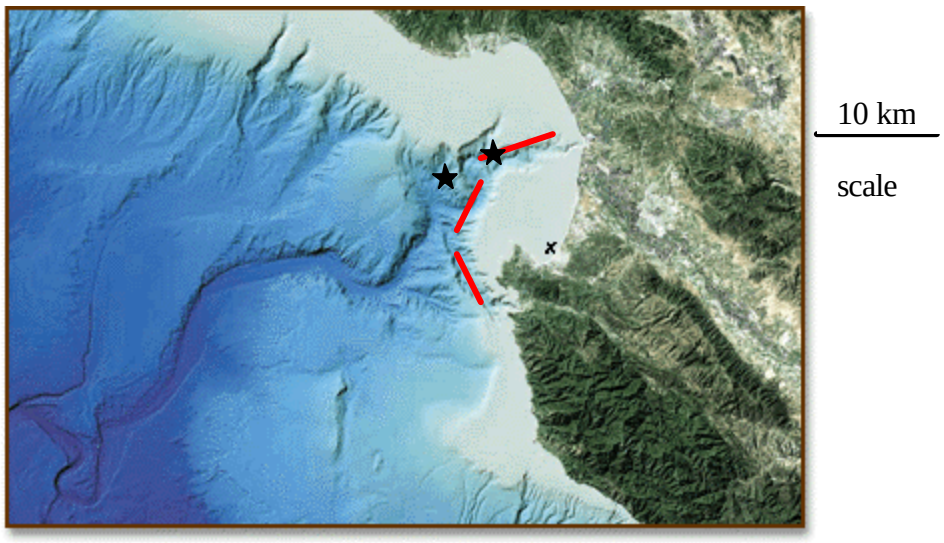

Figure 1. Location of Monterey Inner Shelf Observatory (MISO) site. The Monterey Canyon can be seen bisecting the bay with its steep walls and complex bathymetry. The 'x' denotes the location of MISO and the 3 bars indicate possible generation sites for internal bores. The 2 stars indicate buoys M1 (inshore) and M2 (offshore). Courtesy of MBARI.

distance of 5000m. Roughly linear segments of rapid off-shelf depth changes are indicated in Figure 1 with the shelf break directly offshore approximately 10km northwest of MISO. These three shelf break areas can be considered as potential generation sites for internal tidal bores within the bay.

2. Offshore Ocean Observations

Data collected by the Monterey Bay Aquarium Research Institute (MBARI) was used to characterize the offshore stratification of the bay for the year (2001-2002) previous to the July and August 2002 bottom boundary layer observation made at the MISO site. Temperature, salinity, and pressure from in-situ sensors separated by 20m on the M1 (inshore 36.75^{o}N, 122.03^{o}W) and M2 (offshore 36.70^{o}N, 122.39^{o}W) moorings (Figure 1) were analyzed and used to calculate potential density (s_q). The data were collected at 20 sec intervals and averaged to 2-day samples in this analysis. From this, the potential density was then used to calculate N, the Brunt Vaisala or buoyancy frequency,

$$N = [\frac{g}{r}(\frac{dr}{dz})]^{\frac{1}{2}} \quad (\text{s}^{-1}) \tag{1}$$

d r /dz was calculated using the method of finite differencing. MBARI salinity, temperature, and pressure data were collected every 20m down to depths of 200m (M1) and 300m (M2) at 20sec intervals. These data were linearly interpolated to depths of 10m and used to estimate d r /dz using finite differencing.

$$\frac{dr}{dz} \cong \frac{r_z - r_{z-1}}{z_z - z_{z-1}} \tag{2}$$

where subscript z denotes the depth level and subscript z-1 denotes the level above z. This method, however, has certain limitations. Unfortunately, the 20m sensor spacing of M1 and M2 under samples sharp density gradients with scales << 20m. Therefore, this estimate of N can be regarded as a lower bound. More significant is that the mixed layer can nearly reach the surface, so the 20m depth spacing would not be able to resolve this shallow stratification. Due to this limited vertical sampling, the N calculated here is a

smooth, coarse estimate of the actual stratification; however it does give a long-term timeseries of coarse upper ocean structure.

Together, s_q and N are used to evaluate the seasonal stratification cycle of the bay and to determine if conditions can support the generation of an internal tide and solitary internal waves.

3. Winds

Climatological wind data measured at buoys M1 and M2 show that winds are predominately from the northwest at 5-10 ms^{-1} during most part of the year in Monterey Bay. There are brief interruptions in the daily wind pattern during the winter months due to winter storms moving through the area (Figure 2). The summer period is strongly dominated by persistent northwest winds. Daily wind patterns drive the surface circulation of the bay and have a large effect on surface layer mixing and upwelling sources. Near surface stratification can rapidly change due to a reversal of the winds. When winds are from the north, they transport with them cold, fresh water, in contrast to when they are from the south, when they transport warm, more saline water up towards the bay. Depending on the wind patterns, and direction of the surface currents, the presence of shallow stratification can quickly change. So consequently, winds may impact the formation and propagation of an internal tide and solitons.

Wind forcing during the spring and summer months also plays a significant part in coastal upwelling and the advection of water into and out of the bay (Rosenfeld *et al.* 1993). This too can have a strong impact on the stratification of the bay. Collins *et al.* (2002) noted that surface waters in Monterey Bay were coolest during the spring/summer upwelling period. He also noted coldest temperatures ($<10^{o}$) at 80 dbar during periods of intense upwelling. In contrast, the winter months typically see a decrease in winds from the northwest. Along the coast, upwelling begins to cease and the Davidson current begins to surface (Pennington and Chavez 1999). Winter storms move through the

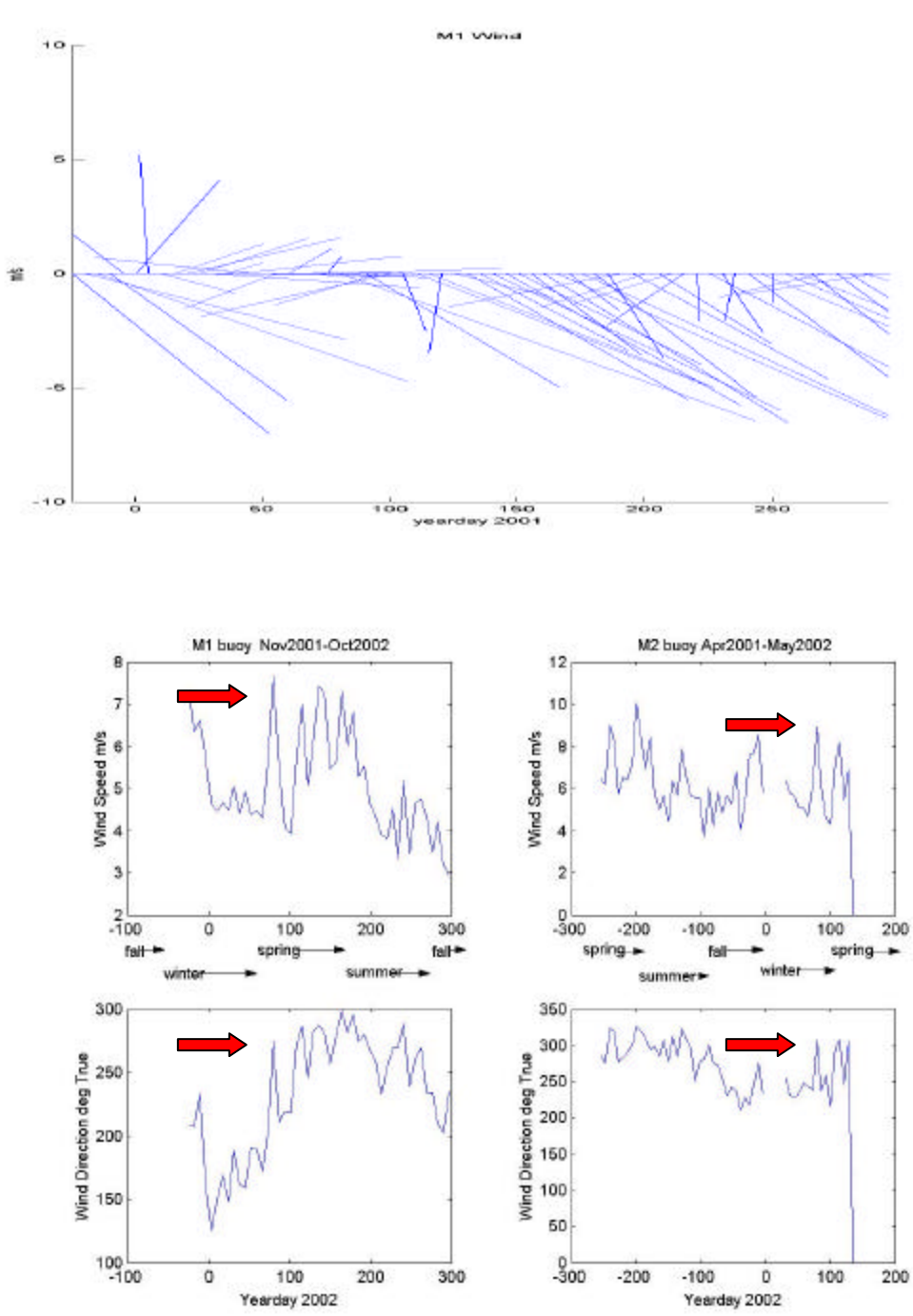

Figure 2. Wind speed and direction from MBARI M1 and M2 buoys. Data is averaged every 7 days over the period of 1 year. Scalar averaging makes winter storms much more apparent as seen by the arrows. During the winter period, these winter storms disrupt the normal wind patterns and help to lower the mixed layer in the water column. They help to mix the upper part of the water column and decrease the insulation. These factors combine to deepen the stratification during the winter.

region, bringing with them intense winds that result in a deepening of the mixed layer. This turbulence decreases the insulating effect in the upper part of the water column. Cessation of upwelling and the start of winter storms combine to decrease the near surface stratification in the bay during the winter months. Collins (2002) identified surface waters to be warmest in the fall and on into the winter. He observed waters below 80 dbar to be warmer during the winter with some temperatures exceeding 14^{o}C. The stratification maximum is typically found deeper in the water column and relatively weaker during the winter period.

4. Circulation

Wind driven currents produce a strong surface circulation within and just offshore of Monterey Bay. Since winds are predominantly from the northwest in the summer, the surface current flows from north to south as it passes the entrance to Monterey Bay. During upwelling conditions, the source of this water is located just north of the bay centered at Pt. Ano Nuevo (Rosenfeld *et al*. 1993). This cold, salty water typically dominates the water mass source in the bay and helps to sustain the strong near surface stratification that is present in the summer. Strub *et al*. and Chelton *et al*. (1987, 1988) have identified a seasonal cycle associated with currents in Monterey Bay. They observed a southward flow during the upwelling season (spring, summer) and a northward flow the rest of the year. During the spring/summer upwelling period the water is cooler at 80 dbar due to a southerly flow in contrast to the winter when water is warmer at the same depth due to a northerly flow.

Within the bay, as winds carry surface water down from the north, surface circulation is observed to move in a counterclockwise direction, advecting the cold, salty water into the bay. Just outside of the bay, the mean surface circulation is in a clockwise direction.

5. Stratification

Stratification during the summer is stronger than in the winter within Monterey Bay as seen daily in sampled temperature and density profile timeseries (Figures 3 and 4). MBARI data show strong, near surface stratification present offshore at M1 and M2 moorings during the summer months. In the summer there are strong near-surface

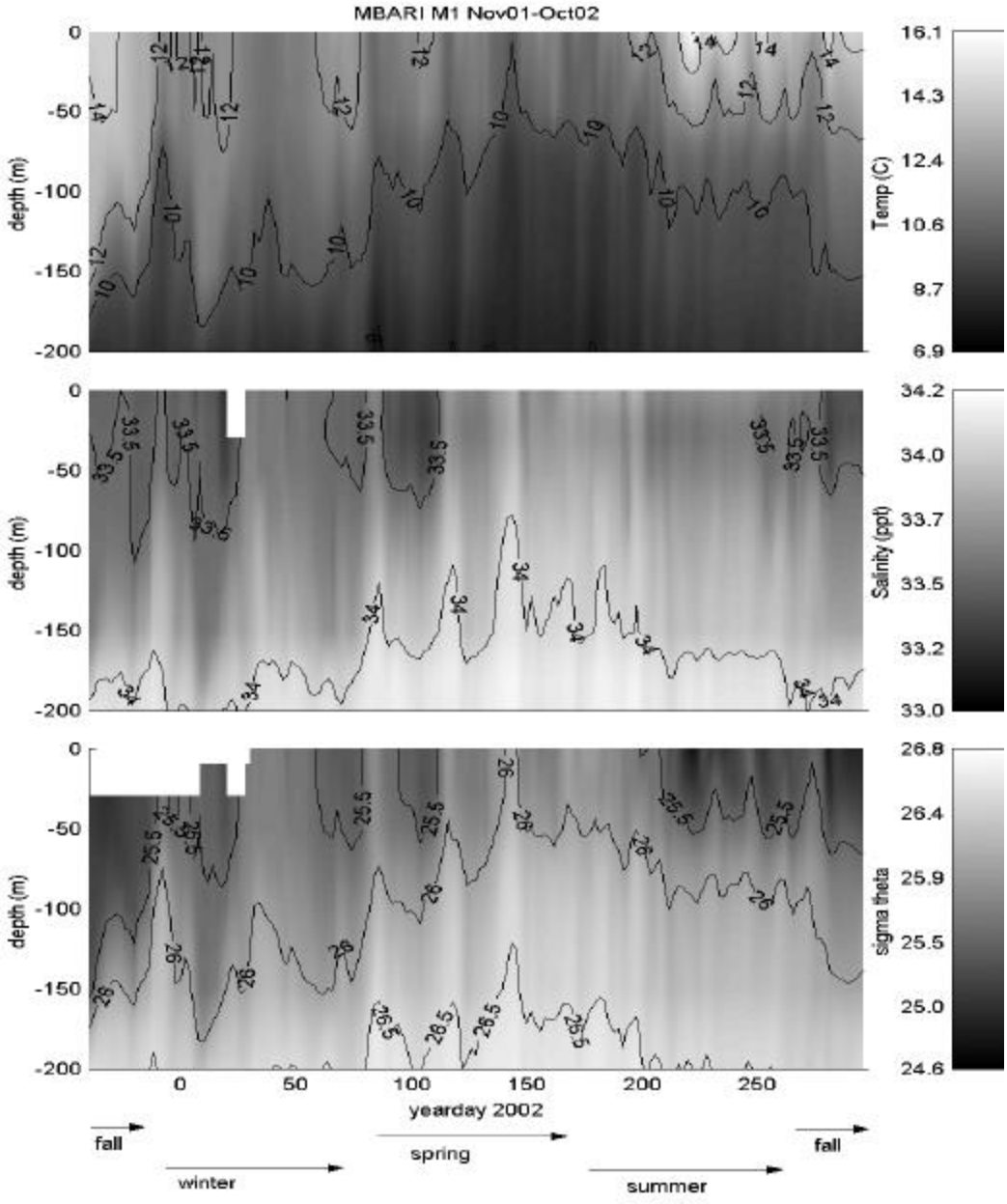

Figure 3. (a) Temperature timeseries of M1 mooring in Monterey Bay. 13Nov01-17Oct02. (b) Salinity timeseries of M1 mooring in Monterey Bay. (c) Sigma-theta (σ_θ) timeseries of M1 mooring in Monterey Bay. Strong, shallow stratification can be seen during the summer months. The winter months show a weaker and deeper stratification. Conditions during the summer months are more ideal for the generation of an internal tide and solitions.

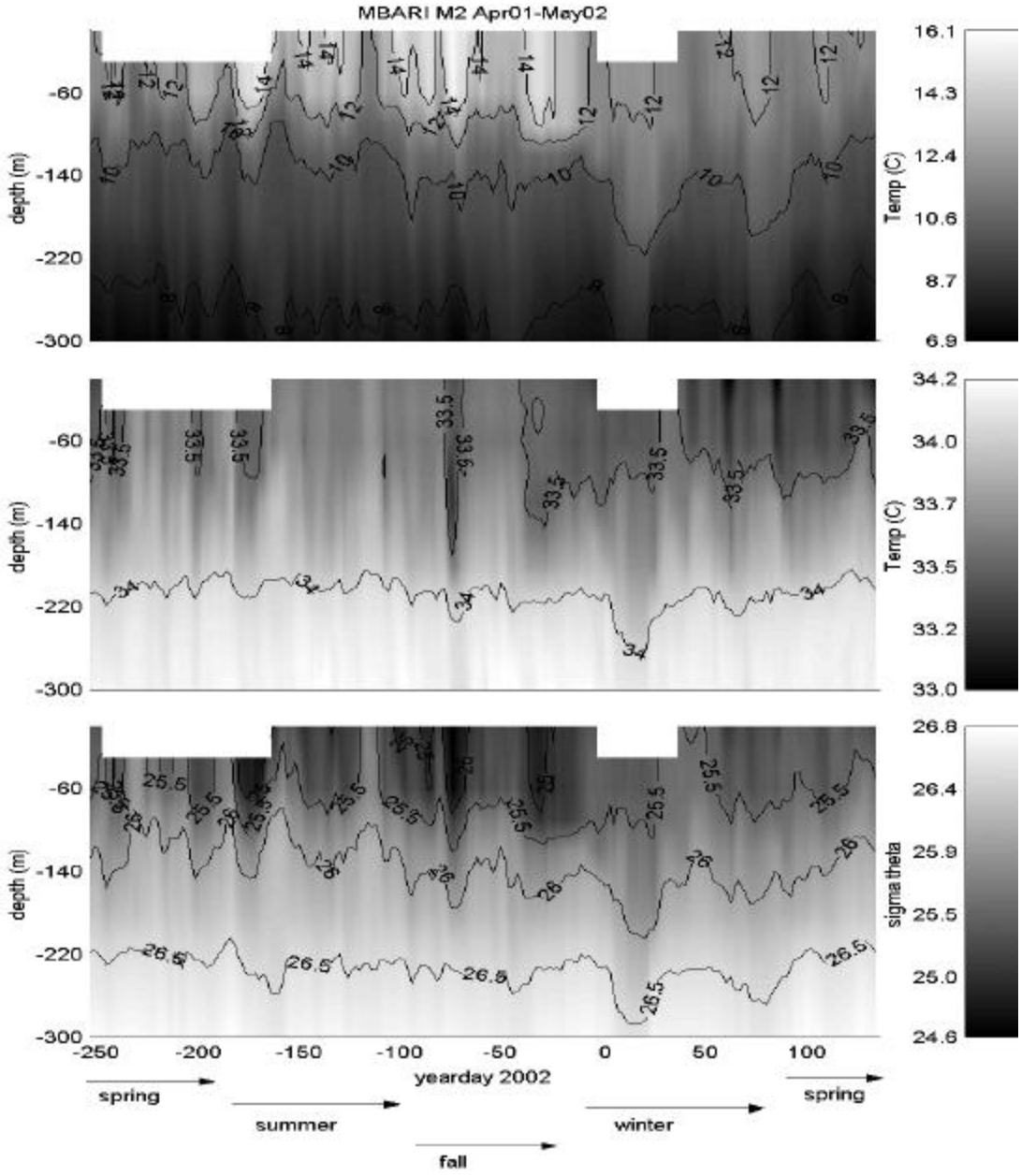

Figure 4. (a) Temperature timeseries of M2 mooring in Monterey Bay. 12Apr01-08May02. (b) Salinity timeseries of M2 mooring in Monterey Bay. (c) Sigma-theta (σ_θ) timeseries of M2 mooring in Monterey Bay. Strong, shallow stratification can be seen during the summer months. The winter months show a weaker and deeper stratification. Conditions during the summer months are more ideal for the generation of an internal tide and solitions.

thermal gradients and the stratification nearly reaches the surface (Figure 5). At M2, strong near surface stratification is observed as well (Figure 6). In each case, thermal gradients extend above 40m depth. Distinct undulations in the warm upper layer can be observed, particularly in the M2 data. This may be associated with changes in forcing during the spring and summer in which the water column restratifies every 2-3 weeks due to a reversal of the winds which interrupts the upwelling conditions. High temperatures and low salinity observed at the surface both contribute to a strong near surface stratification. Profile timeseries of salinity and potential density for M1 and M2 are similar in structure to the thermal structures in Figures 5 and 6. Figures 5 and 6 clearly show the strong density gradients that are present near the surface during the summer. The summer months distinctly show the presence of a strongly stratified water column near the surface, which approximates a two-layer system. However, due to the 20m sensor spacing on the M1 and M2 moorings, the density structure is unable to be resolved to finer scales. This limits our estimate of the Viasalla frequency to a lower bound, and prevents a definition of mixed layer depth.

During the winter months, however, near-surface stratification disappears almost completely (Figures 7 and 8). At both the M1 and M2 moorings, stratification is weaker and located much deeper in the water column. The deeper mixed layer during the winter is due to an increase in surface stress from winter storms and the cessation of upwelling. Despite having low average winds, strong, intermittent winter storms help to deepen the mixed layer with sudden increases in colder winds. Because Figure 2a is a vector average over 1 year, winter storms would have a weak signature, as they are episodic, multi-directional events. However, when scalar wind speeds are averaged, the winter storms become much more apparent (Figure 2). The winter months also show the absence of a near-surface salinity stratification, indicating that the mixed layer is deeper in the water column as seen in Figures 7 and 8.

Profile timeseries of N (Brunt-Visailla frequency) vs. depth help to determine the strength of the water column stratification. Strong stratification near the surface, seen in the summer average (Figures 5 and 6), produced a lower bound N_{max} value of 0.014 s^{-1} at a depth of 50-60m. Weaker stratification, which is seen in the winter, yields values of

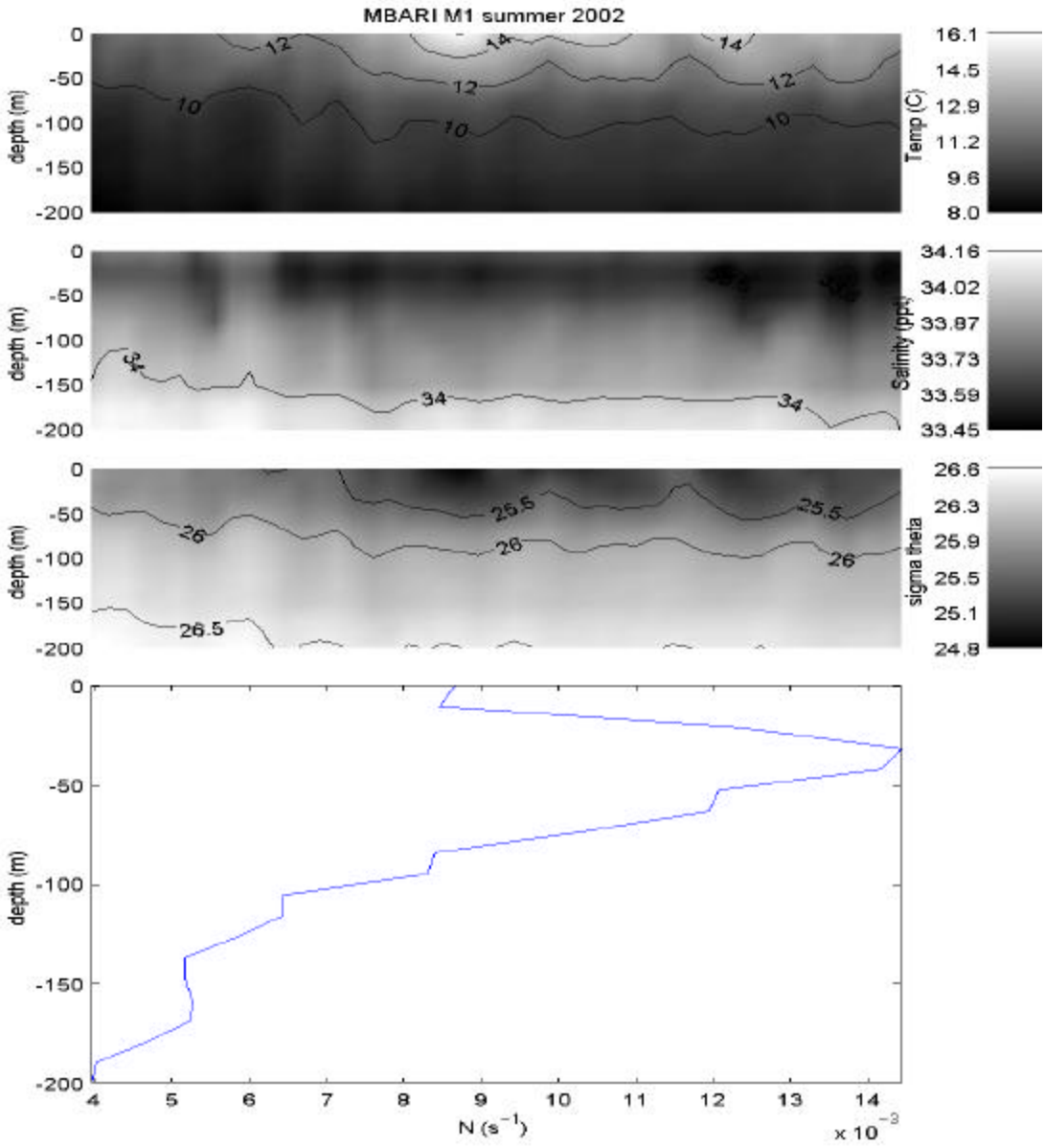

Figure 5. Summer conditions at M1 mooring in Monterey Bay for yearday 172 to 266. (a) Temperature profile indicates a strong and shallow stratification in the water column. (b) Salinity profile shows a strong and shallow stratification as well. (c) Sigma-theta (σ_θ) profile agrees well with the temperature and salinity profiles showing a strong and shallow stratification. (d) N (buoyancy frequency) calculated as a summer mean using 20m σ_θ differences gives indication that shallow stratification is occurring in the water column. The strong, shallow stratification in the summer is ideal for the generation of an internal tide and solitons.

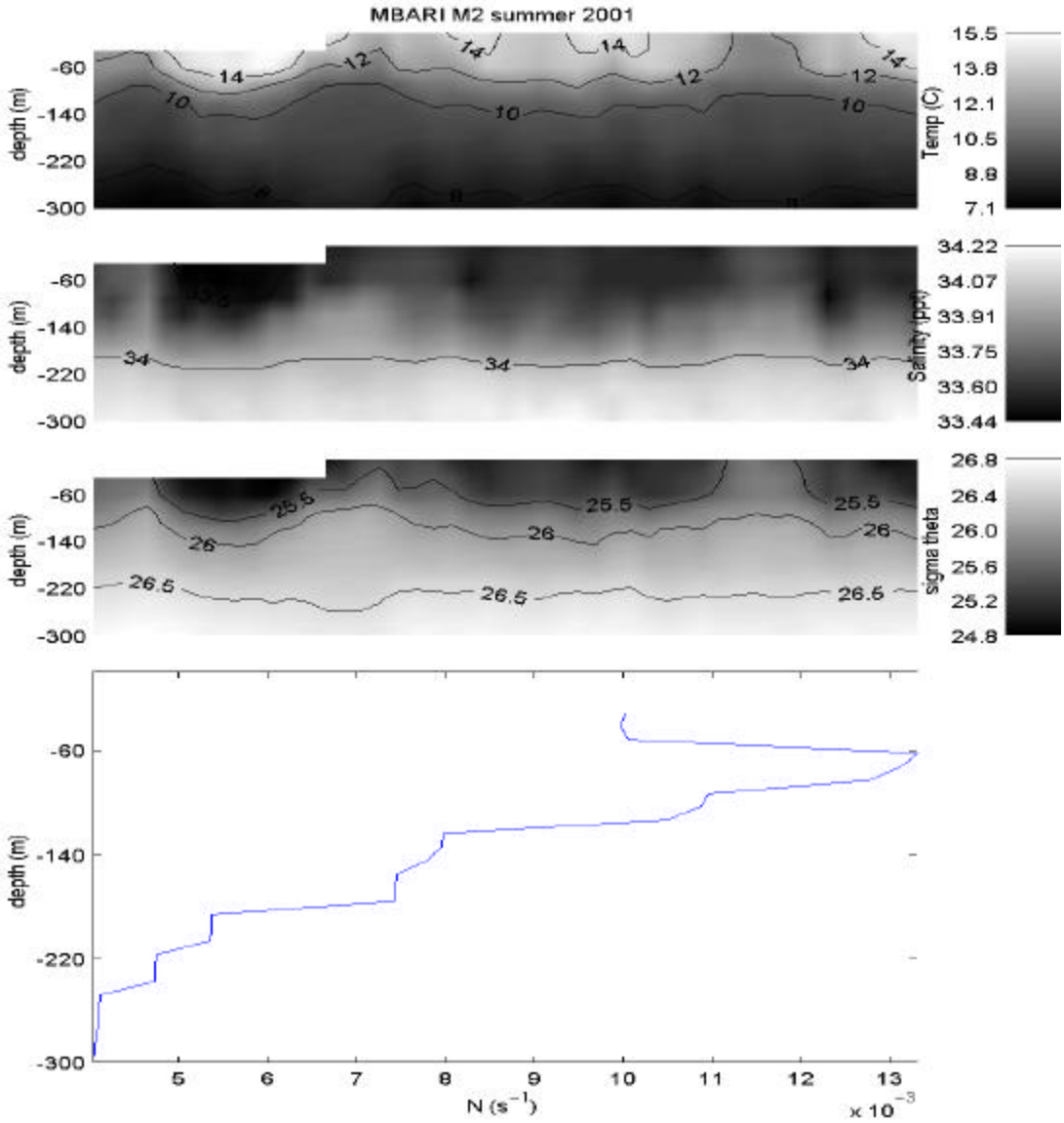

Figure 6. Summer conditions at M2 mooring in Monterey Bay for yearday 172 to 266. (a) Temperature profile indicates a shallow and strong stratification in the water column. (b) Salinity profile shows a strong and shallow stratification as well. (c) Sigma-theta (σ_θ) profile agrees well with the temperature and salinity profiles showing a stronger and shallower stratification. (d) N (buoyancy frequency) calculated as a summer mean using 20m σ_θ differences and plotted vs. depth confirms that the water column has a very strong and shallow stratification. The strong, shallow stratification in the summer is ideal for the generation of an internal tide and solitons.

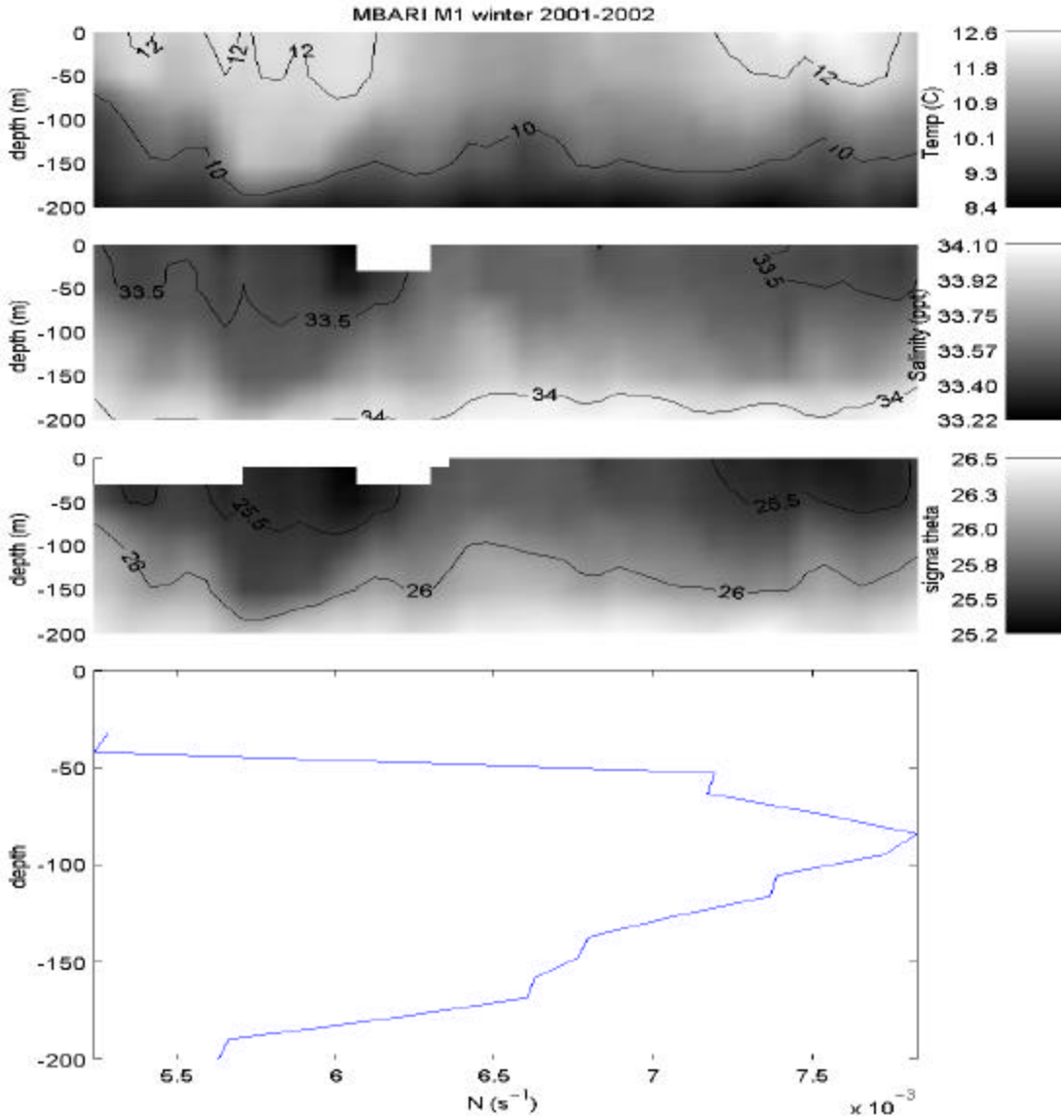

Figure 7. Winter conditions at M1 mooring in Monterey Bay for 2001-2002 yearday 356 to 80. (a) Temperature profile indicates a very deep and weak stratification in the water column. (b) Salinity profile shows a deeper stratification as well. (c) Sigma-theta (σ_θ) profile agrees well with the temperature and salinity profiles showing a deep and weak stratification. (d) N (buoyancy frequency) calculated as a winter mean using 20m σ_θ differences plotted vs. depth clearly indicates that stratification is weak and occurs very deep within the water column. The weak, deep stratification in the winter is not ideal for the generation of an internal tide and solitons.

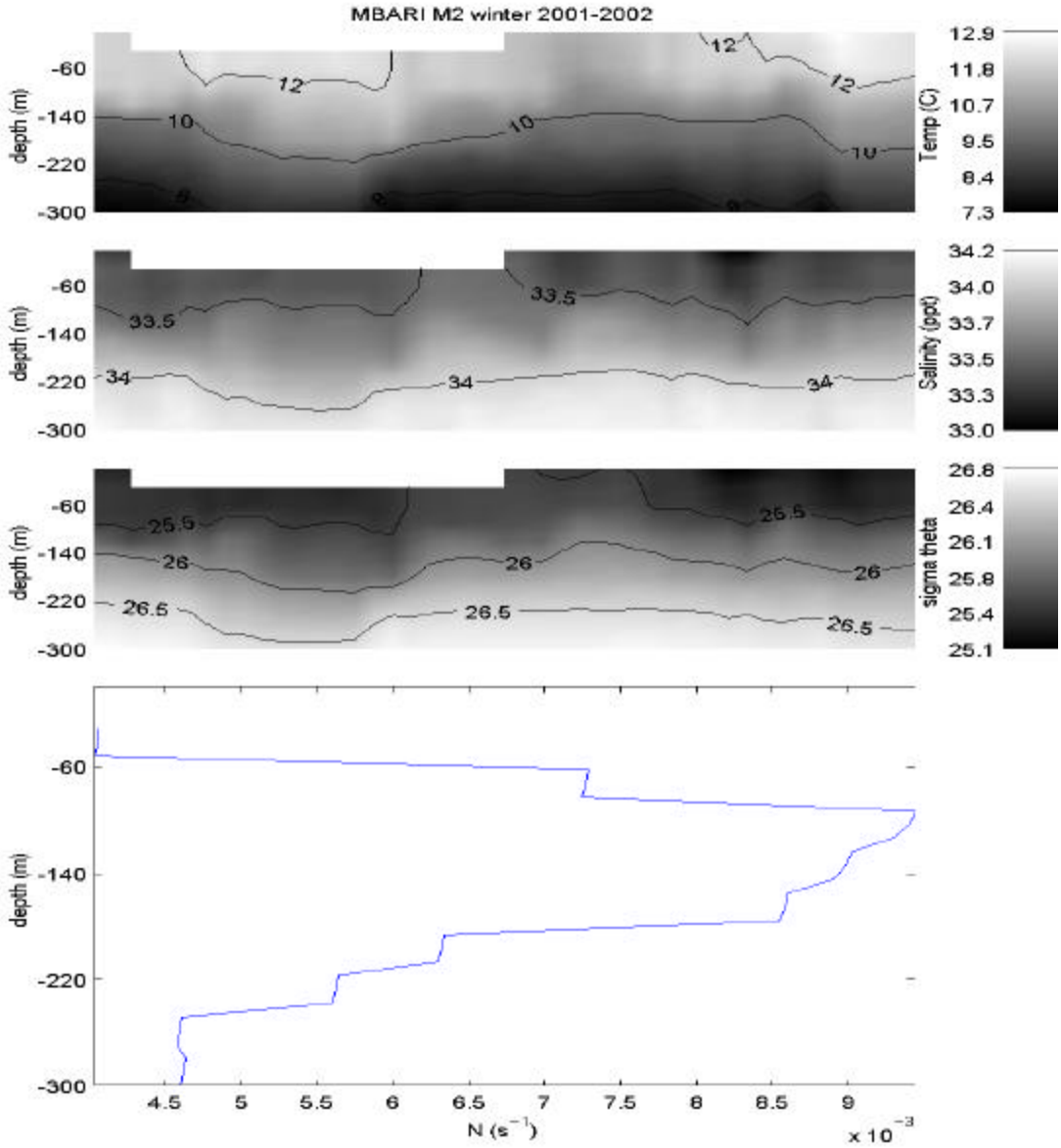

Figure 8. Winter conditions at M2 mooring in Monterey Bay for 2001-2002 yearday 356 to 80. (a) Temperature profile indicates a very weak and deep stratification in the water column. (b) Salinity profile shows deeper stratification as well (c) Sigma-theta (σ_θ) profile agrees with the temperature and salinity profiles indicating that the water column has a weak and deep stratification. (c) N (buoyancy frequency) calculated as a winter mean using 20m σ_θ differences plotted vs. depth clearly indicates that stratification is present, but very deep in the column. The weak, deep stratification in the winter is not ideal for the generation of an internal tide and solitons.

N_{max} on the order of 0.008 s^{-1}, significantly less than those of summer months. These values of N_{max} are generally found deeper in the water column at a depth of 80m (Figures 7 and 8).

Together these timeseries give a clear indication that the water column during the summer has a strong, near surface stratification. This makes conditions during the summer more ideal for the generation of an internal tide and solitons. Because the MBARI data have limited resolution of the water column due to its 20m sensor spacing, CTD data were taken from NAVO sponsored Calcofi cruises within Monterey Bay in order to validate and support our conclusions on the stratification. The 1000m CTD casts from July 2000 and August 2001 show a finer resolution of the strong near surface stratification. Conversely casts from February 2001 and January 2002 near the mooring sites show deeper, weaker stratificaiton. These CTD casts provide a 2m resolution of the temperature, salinity, and density structures. The CTD casts were made in the vicinity of the M1 mooring at 36.73°-36.74°N and 122.028°-122.026°W. Figures 9 and 10 show the CTD casts in which vertical profiles of temperature, salinity, density anomaly, and N were computed. Figure 9 depicts the summer conditions, showing a mixed layer at 1-2m depth for July 2000 and at 10m depth for August 2001, whereas Figure 10 depicts the winter conditions with a mixed layer at 50m for February 2001 and January 2002. When compared with N, we can see better resolved values of the stratification, with N_{max} for the summer of 0.03 s^{-1} near the surface at 1-2m depth. This value is considerably larger than N_{max} for the winter which had a value of 0.015 s^{-1} at a depth of 60m.

6. Tides

A barotropic semidiurnal tide is present in Monterey Bay, resulting in two highs and two lows that occur daily. The tides are linked to astronomical forcing dominated by the position of the sun and moon relative to the earth. During the summer, the new and full moons generally fall around the middle and end of each month, with each month changing slightly due to the lunar cycle and sidereal day versus the calendar day. respectively. It is at these times when the earth, sun, and moon are aligned that the tides are very large and are known as spring tides. When the moon is in first or last quarter (beginning and third week of each month), the tides are generally weaker and are known as neap tides. These tides occur when the earth, sun, and moon are in quadrature. Spring

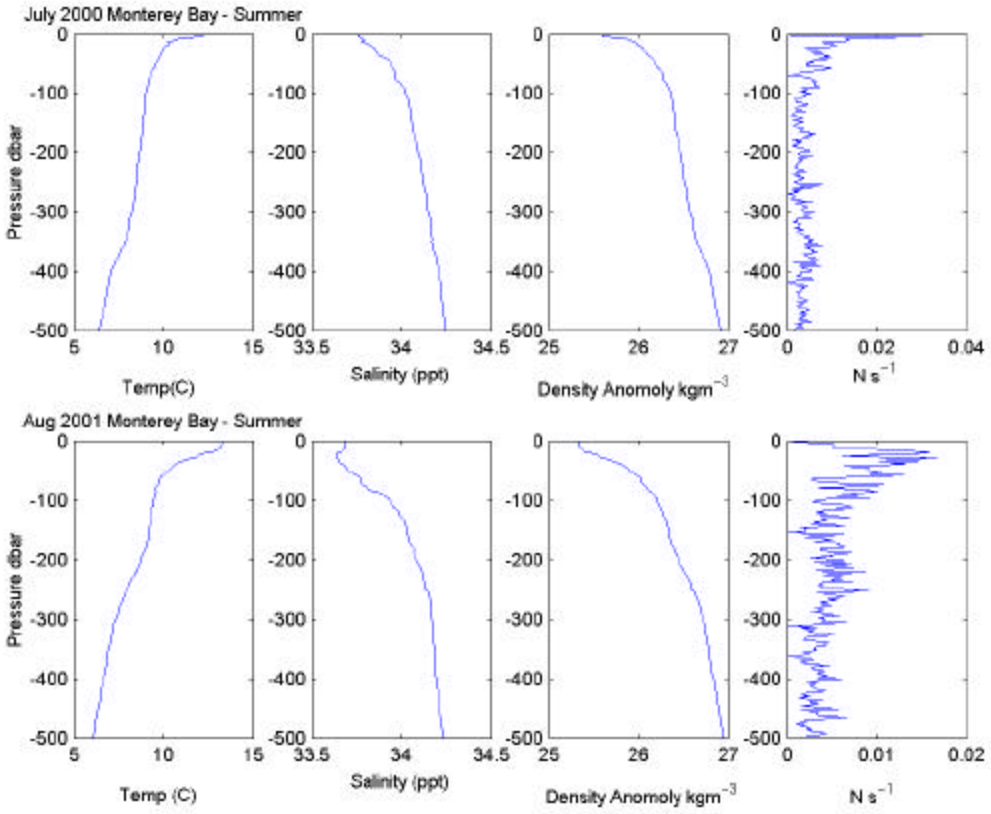

Figure 9. CTD data taken from NAVO sponsored Calcofi cruises. Location of cast: 36.74°N, 122.027°W. (a) July 2000. Strong, shallow stratification is clearly observed in the Temperature and Density Anomaly vertical profiles. The mixed layer can be observed at 1-2m depth. N vs. depth shows Nmax occurring at the surface (1-2m) with a magnitude of 0.03 s^{-1}. (b) August 2001. During late summer, stratification starts to move deeper into the water column. It can be found at 10m depth. Nmax is also seen to decrease to 0.015 s^{-1} and move down as well (10m). Summer conditions show a very strong, near surface stratification occurring within the water column, ideal for internal tide generation and evolution of solitons.

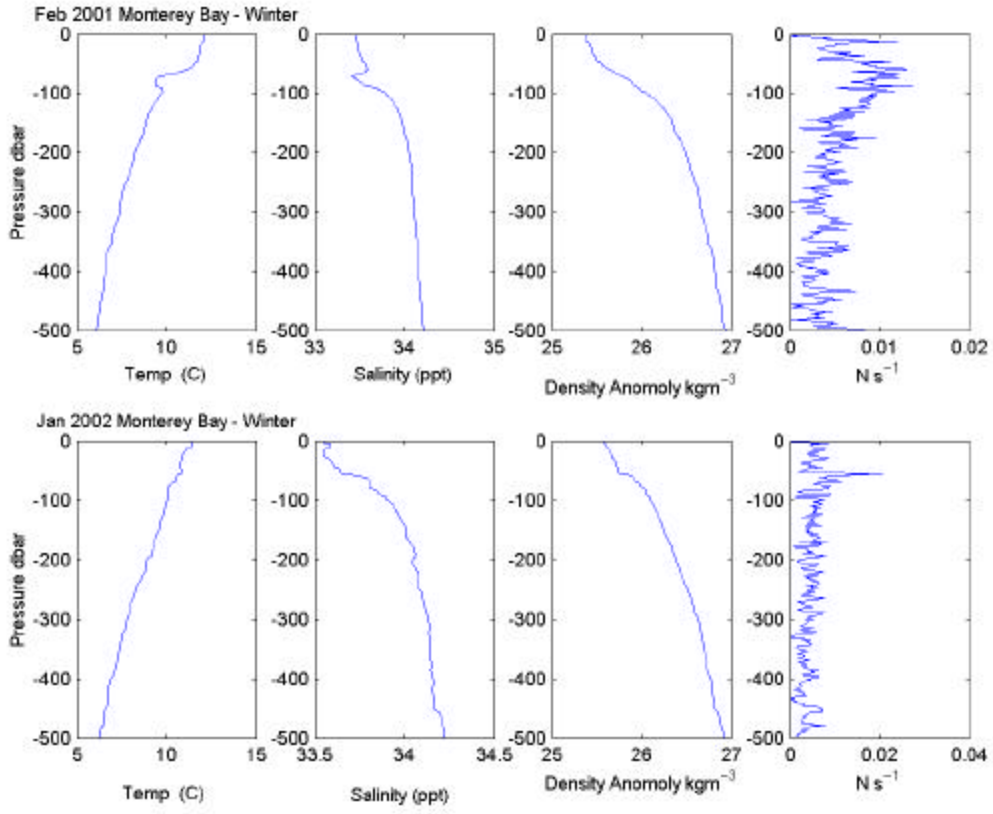

Figure 10. CTD data taken from NAVO sponsored Calcofi cruises. Location of cast: 36.74°N, 122.027°W. (a) February 2001. Weak, deep stratification is clearly observed in the Temperature and Density Anomaly vertical profiles. The mixed layer can be observed extending down to 50m depth. N vs. depth shows Nmax occurring much at 50m with a magnitude of 0.01 s^{-1}. (b) January 2002. The Temperature and Density Anomaly vertical profiles identify an almost non-existent mixed layer at approximately 60m. Again, Nmax defines the mixed layer at 60m with a magnitude of 0.02 s^{-1}. Winter conditions show a very week, deep stratification in the water column, not ideal for the generation of an internal tide and solitons.

tides have offshore tidal surface currents up to 20 cms^{-1}, while neap tides have tidal surface currents up to 10 cms^{-1}, as observed by Petruncio (1993) and Paduan *et al.* (1995) using CODAR. They observed tidal surface currents to be larger at the head of the canyon (15 cms^{-1}) and to be aligned with local bathymetry at the southern end of the bay. The K1 and O1, which are the lunisolar diurnal constituents that expresses the moon's declination, have periods of approximately 24 hours (NOAA). The M2 and S2, which are the principal lunar and solar semidiurnal constituents, have periods of approximately 12 hours. Together, each of these tidal constituents contributes to over 80% of the total amplitude and tidal forcing in Monterey Bay.

A barotropic semidiurnal tide dominates the bay and is characterized as a surface wave with particle motion following the high and low tides. Theses tides have extremely long wavelengths on the order of thousands of kilometers. The astronomical forcing of M2 was observed to be the strongest, contributing the most to the barotropic tidal activity within the bay (Petruncio *et al.* 1997). The second strongest constituent observed was the S2, which was 26% of M2.

7. Internal Tide Generation Mechanisms

With a strong, shallow stratification present, a sharp shelf break 10km offshore, and a strong barotropic cross-shelf current, conditions in Monterey Bay are ready for the generation of an internal tide. The internal tide is generated in the following manner, following Chapman et al (1997):

As the ebb tide begins to flow out of the bay and makes contact with the shelf break, it causes a depression in the isopycnals (Figure 11a). This isopycnal depression, or thickening of the upper layer of the stratified column, is the result of a standing lee wave formed by offshore flow over the hydraulic jump at the shelf break. When the flow ceases during slack tide, the pycnocline depression is able to propagate internal tidal bores both onshore and offshore (Figure 11b). During the flood tide, the steep edge onshore bore propagates shoreward (Figure 11c) (Holloway 1987). The leading edge of this internal bore will begin to steepen due to dispersion effects as the bore continues to propagate shoreward. Nonlinearities will begin to arise as the leading edge continues to become steeper. These nonlinearities are what give rise to solitons (Figure 11d) (Liu

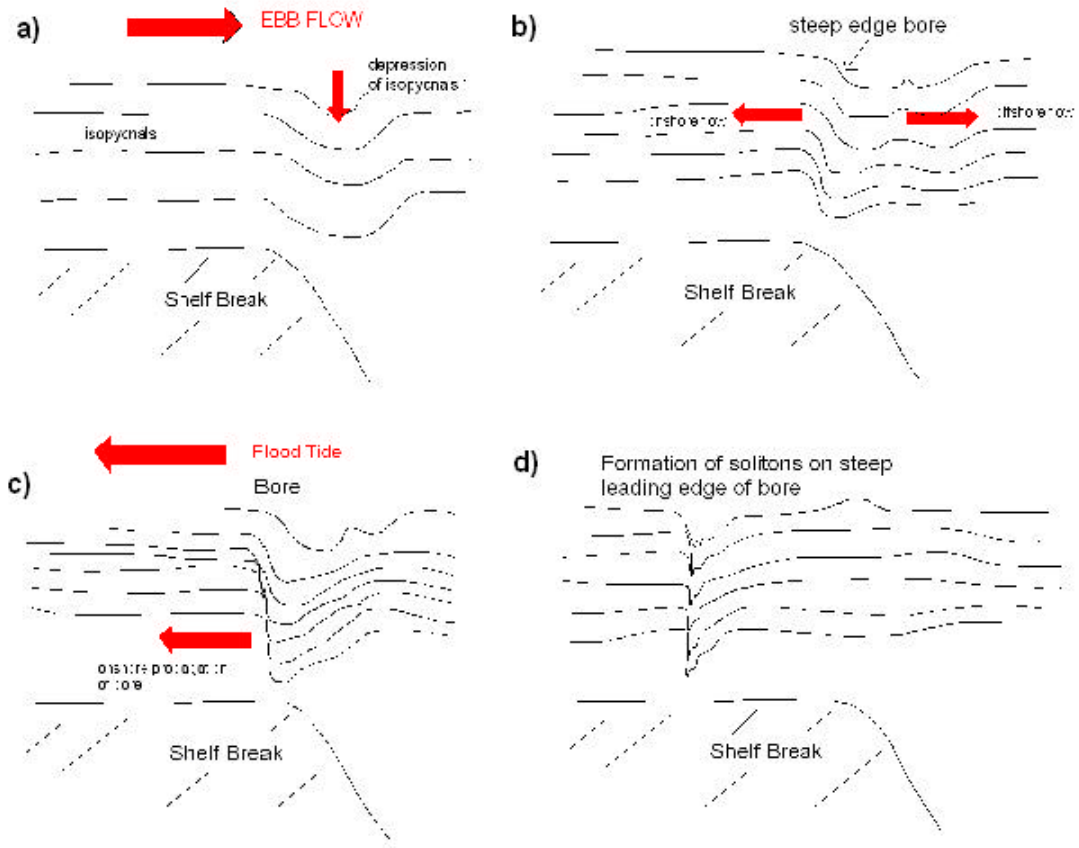

Figure 11. (a) Ebb flow across a shelf break causes a depression in the pycnocline. (b) Formation of a steep edge shoreward bore during slack tide. (c) Internal bore propagates shoreward assisted by the flood tide. Leading edge continues to steepen due to dispersive effects. (d) The steep leading edge of the bore degenerates into solitons through the dispersive properties of internal waves.

1988). As the internal tidal bore continues propagating shoreward across the shelf, the solitons begin to grow in size and energy.

The generation of an internal tide is closely related to the slope of the shelf break and tidal forcing of the M_2 and S_2 frequencies (Baines 1982). The rate of conversion of surface tidal energy into internal tidal energy is most notable over continental slopes and increases rapidly with the topographic height (Baines 1972). Baines (1985) modeled internal tide generation in laboratory experiments as a function of the amplitude of the barotropic tidal forcing given by the Froude Number, $F = \frac{u_{sb}}{c_w}$, where u_{sb} is the maximum barotropic tidal velocity at the shelf break and c_w is the long wave speed of the lowest internal mode. He found a strong correlation between the slope of the shelf and the Froude number. For a two-layer stratification, large Froude numbers (>1) were observed indicating that linear wave theory was not adequate to predict internal tide generation over the hydraulic jump that occurs seaward of the shelf break during the ebb phase of the barotropic tide. However, in his laboratory experiments, he was able to conclude that for high Froude numbers and steep slope geometry, a hydraulic jump will form seaward of the shelf break during the ebb phase of the tidal cycle. For an approximate 2-layer stratification with one layer thicker than the other, an internal bore will form. Values of F>1 are commonly seen in the open ocean over continental shelves and help to explain the nonlinear character of internal waves of tidal origin (Baines 1985).

Holloway (1999) also came to the conclusion that internal tide generation is strongly dependent on the relationship between the slope of the bathymetry and the slope of the internal wave characteristics. He defined the slope characteristics (s) as the path along which the wave energy propagates as $s = \frac{+}{-}\sqrt{\frac{w^2 - f^2}{N^2 - w^2}}$, where w is the wave frequency, f is the Coriolis parameter, and N is buoyancy frequency. He further defined critical values for bathymetry slope (a): critical when $\frac{a}{s}$=1, subcritical when $\frac{a}{s}$<1,

and supercritical when $\frac{a}{s}$>1. He observed that little generation occurs for weak subcritical slope, while resonance near the sea bed may occur for critical slopes.

The continental shelf break 10km directly offshore of the MISO site, as well as the southern wall of the Monterey Canyon to the north, are shelf breaks for the generation of an internal tide within Monterey Bay. Because the continental shelf break is directly offshore and parallel to the coast, it will produce internal bores that propagate in a cross-shore (CS) direction, whereas internal tidal bores generated along the southern wall of the canyon would likely produce more alongshore (AS) directed bores that could be refracted by the shallow, inner shelf topography.

B. SOLITONS

Solitons move in packets frequently bound to the steep front of an internal tidal bore. They are widely observed in coastal regions when the water column is stratified and generally propagate CS and can be found to be moving on and offshore (Apel 1983). They are strongly nonlinear internal waves that are coupled with the internal tide and generate strong current pulses in the water column.

Solitons can be characterized by their large amplitudes, vertical displacements of the isotherms, and strong currents associated with them. They are commonly observed as part of a wave train on the leading edge of the steepening internal bore and are readily identified by the vertical alignment of current and isotherm displacements (Liu 1988). In a very strongly stratified coastal region, Stanton and Ostrovsky (1998) observed vertical displacement amplitudes of a soliton to be 2-4 times greater than the pycnocline depth with lateral currents up to $1ms^{-1}$ off the coast of Northern Oregon. Within these wave packets, there are rapid, unidirectional pulses in the direction of propagation of the solitons. In a coastal region with much weaker stratification, Chapman et al (1997) observed typical speeds of $1\text{-}2cms^{-1}$, with some peaks as great as $5cms^{-1}$. They also noted large temperature variations of up to 6-7°C within the New York Bight. In both these regions a distinct shelf break was located offshore of the solitary internal wave observation site, similar to the topographic structure in the southern part of Monterey Bay.

When the leading edge of the internal bore steepens due to dispersion effects, the amplitude of the solitons increases as well. As the amplitude increases, the width of the soliton decreases (Stanton and Ostrovsky 1998). Increasing order of nonlinear functions are then needed to describe their structure. Stanton and Ostrovsky (1998) defined the width of a soliton as the time interval between displacements at half the maximum amplitude. Solitons off northern Oregon were observed to have durations of 180s. For the 25 solitons observed, Stanton and Ostrovsky (1998) noted that as the amplitudes varied from 25m to 5m, the durations (and here widths) remain generally unchanged at 180s.

Soliton displacement can occur near the surface or near the bottom of the water column depending on the background stratification, which is itself modulated by the internal tide on the inner shelf. As a near surface soliton propagates shoreward and begins to shoal, its form changes and may affect the bottom boundary. Liu (1988) notes that as the wave train propagates inshore from the shelf break at a depth of 90m to the nearshore observation site at a depth of 30m, the linear wave speed is reduced to one-half its initial value, dispersive effects decrease as the wave is compressed, nonlinear effects decrease, and shoaling increases. Liu (1988) also observed that a critical depth existed at 45m depth in the NY Bight at which point the wave packet propagates onto the shelf and disappears. From this, he concluded that varying depth on the evolution of solitons fell into two categories: 1) The linear wave speed is modified along the path of wave propagation that leads to spreading out or compression of the waves that disintegrate into a dispersive wave train at the critical depth. 2) The slope of the shelf produced a shoaling term proportional to the wave amplitude. This shoaling was observed to increase the soliton's amplitude and increase the wave energy. However, Liu (1988) also noted that turbulent processes begin to erode the peaks of the well-developed soliton, decreasing their amplitude, and increasing their width. The radial spreading and dissipation effects eventually suppressed the shoaling effects and it was found that the evolution of solitons was a balance between nonlinear and dispersive effects. The eddy viscosity present eroded the sharp peak of the lead soliton causing it to decay, while the shoaling effect balanced the dissipation effect for the rest of the solitons in the wave packet allowing them to grow.

II. FIELD EXPERIMENT

A. PHYSICAL SETUP

The field data used in this study are collected at the Monterey Inner Shelf Observatory (MISO) site, which is part of the Rapid Environment Assessment Laboratory (REAL), located off of Del Monte Beach and the Naval Postgraduate School (NPS) in the southern end of Monterey Bay. MISO was designed and implemented by Tim Stanton and his research group at NPS. It is sponsored by the Oceanography Department at the Naval Postgraduate School and by the Office of Naval Research as part of the Coastal Processes and Physical Oceanography programs and the Shoaling Waves Experiment. The facility was deployed in January 2000 and is ongoing. The inner shelf soliton experiment was a two-month study that took place during the 2002 summer, with rapid CTD profiles supplementing the detailed current measurements for 2 weeks within the period.

The MISO instrument frame is located 600m offshore from the beach in 12m of water and 1m above the bed (Figure 1). Long timeseries of high resolution measurements made on the MISO frame are possible because of the high bandwidth data communications and power links between MISO and the laboratory onshore. These instruments are being used to study the interaction of winds, waves, and sediment bed on the inner continental shelf, just offshore from the surf zone. A detailed diagram of the frame and instruments is shown in Figure 12.

B. INSTRUMENTS

1. Paroscientific Pressure Transducer

A high precision digital pressure sensor (Paro-scientific) measures the height of water above the frame by sensing the hydrostatic pressure of the water column and propagating waves to produce a record of tides and surface gravity waves. It is located approximately 1.2m above the bed. In this study, 5 minute averages of pressure are used to filter out surface gravity waves. The pressure sensing element in this instrument is an oscillating quartz crystal that provides very high long term stability and resolution.

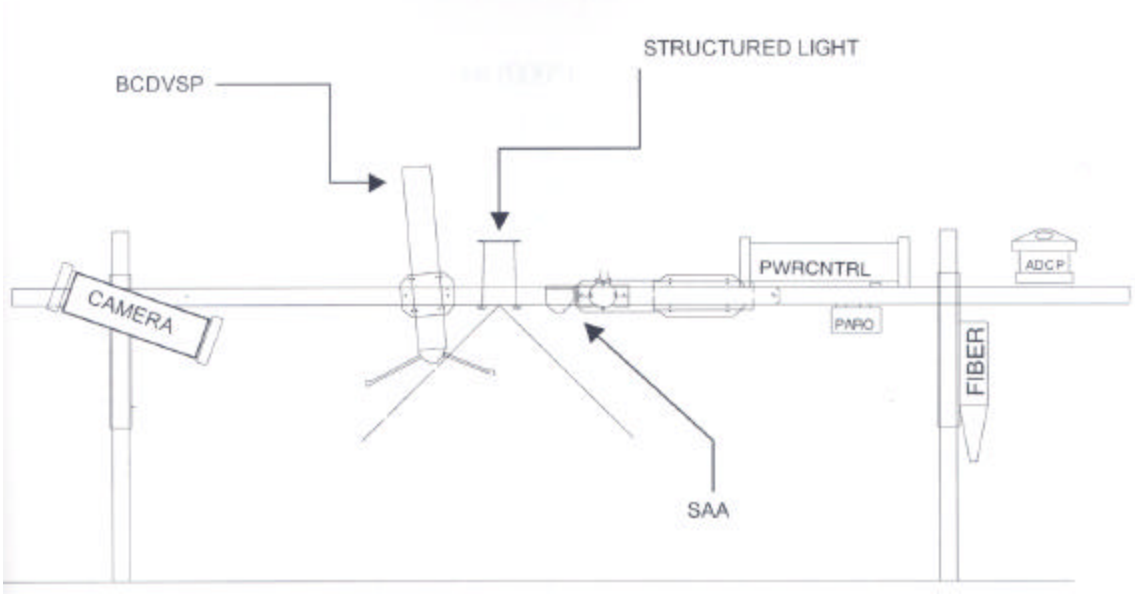

Figure 12. MISO instrument frame as viewed from offshore looking onshore. The instruments include (from left to right): camera component of the Structured Light and Camera (SLAC), Bistatic Coherent Doppler Velocity and Sediment Profiler (BCDVSP), structured light component of the SLAC, Scanning Acoustic Altimeter (SAA), Paro-scientific pressure sensor, and Braodband Acoustic Doppler Current Profiler (BADCP).

2. ADCP

An upward looking WorkHorse Acoustic Doppler Current Profiler (ADCP) manufactured by RD Instruments measures the water current every 0.5m over 27 equally spaced bins from the frame to the near ocean surface. The ADCP starts each ping cycle by transmitting a broadband acoustic pulse into the water column along each of the four narrow acoustic beams that are tilted 20^{o} off the vertical. Each transducer detects Doppler shifts of scatterers in the water column moving with a component of velocity aligned with the beam direction. These Doppler shifts are estimated every 0.5m in the MISO setup by range-gating the signals. The resulting set of four radial Doppler shifts at each range bin are then resolved into three components (u, v, w) of velocity assuming there is no variation in velocities across the diverging beams. This limits the accuracy for wind wave-induced velocities at the most distant bins near the surface; however, in this study lower frequency motions are being considered. Acoustic reflection caused at the surface frequently results in contamination of the upper 1-2 bins. The ADCP is also

equipped with a heading and tilt sensor allowing the instrument coordinates to be transformed into earth-leveled, North referenced coordinates.

3. BCDV

A high resolution Bistatic Coherent Doppler Velocity and Sediment Profiler (BCDVSP) developed at NPS by the ocean turbulence research group measures the three component velocity vector and sediment concentration every 0.01m over 100 equally spaced bins from a range of 0.60m above the bed (Stanton 1999). The BCDV transmits a 1.25MHz acoustic signal, and uses coherent sampling and a bistatic geometry to receive backscattered energy. The BCDV backscatter energy is proportional to the sediment concentration, over a range of from 0.01 to 100g/L. These small- scale measurements are used to define the mean and turbulent structure of the water column above the sandy bed, which results from currents interacting with the bed.

4. CTD

A Direct Reading Micro CTD developed by Falmouth Scientific Inc. was used to collect temperature, salinity, and pressure data over 127 bins equally spaced every 0.1m. Conductivity was measured through a FSI inductive cell with an accuracy of +/- 0.002 S/m and temperature was measured with a platinum resistance thermometer with an accuracy of +/- 0.002^{o}C. Pressure was measured through a micro-machined silicon pressure sensor with an accuracy of +/- 0.02%. An automated, computer controlled winch developed at NPS repeatedly profiled the CTD from 2m HAB to the surface every 2 minutes. The CTD provided temperature and salinity profile timeseries to measure the evolution of the stratification of the water column. Poor temporal response of the conductivity cell severely limited the vertical resolution of the conductivity, and hence, salinity profiles during these observations. Consequently, isotherm displacements are used instead of isopycnals in the following analysis.

5. Meteorology

Wind speed and direction from the Marine Operations Lab MET instrument tower were used as a measure of the local winds. The 8m tower was located approximately 700m directly shoreward of the MISO array.

THIS PAGE INTENTIONALLY LEFT BLANK

III. DATA PROCESSING

A. COORDINATE TRANSFORMATION

In order to correctly analyze the field data collected by these instruments, the coordinate system of the ADCP and BCDV were resolved to a cross-shore (CS) normal coordinate system with +x offshore and +y along-coast toward Monterey (see map, Figure 13). The ADCP is oriented such that it is in magnetic coordinates where +/-**u** is east/west and +/-**v** is north/south. The ADCP heading ($ADCP_{hdg}{}^{o}$) measured by the internal compass was 309^{o}-312^{o} magnetic. Shore normal to the beach was estimated to be 320^{o} magnetic. To provide a coordinate system with +x offshore, -x onshore, and +y alongshore (AS) towards Monterey, and –y alongshore (AS) towards Marina, the ADCP heading must be rotated an additional -90^{o} (Figure 1)

$$\text{ADCP rotation}^{o} = ADCP_{hdg}{}^{o} + (320^{o} - ADCP_{hdg}{}^{o}) - 90^{o} \qquad (3)$$

The BCDV is oriented in a frame coordinate system, 218^{o} from magnetic North, with a heading of 308^{o} magnetic. A 12^{o} rotation had to be applied to resolve it to a shore parallel coordinate system. To further resolve it to a CS normal coordinate system, a -90^{o} was applied to the data.

$$\text{BCDV rotation}^{o} = 12^{o} - 90^{o} \qquad (4)$$

To analyze the effects of wind forcing, wind data had to be resolved into the CS normal system as well. Wind from the onshore MET tower was measured in a north-south coordinate system in degrees True. Because the wind was measured in a true coordinate system a 15^{o} correction had to be made for the magnetic variation. Wind speed and direction were used to calculate the u and v components of the wind. These components were then transformed into the CS normal coordinate

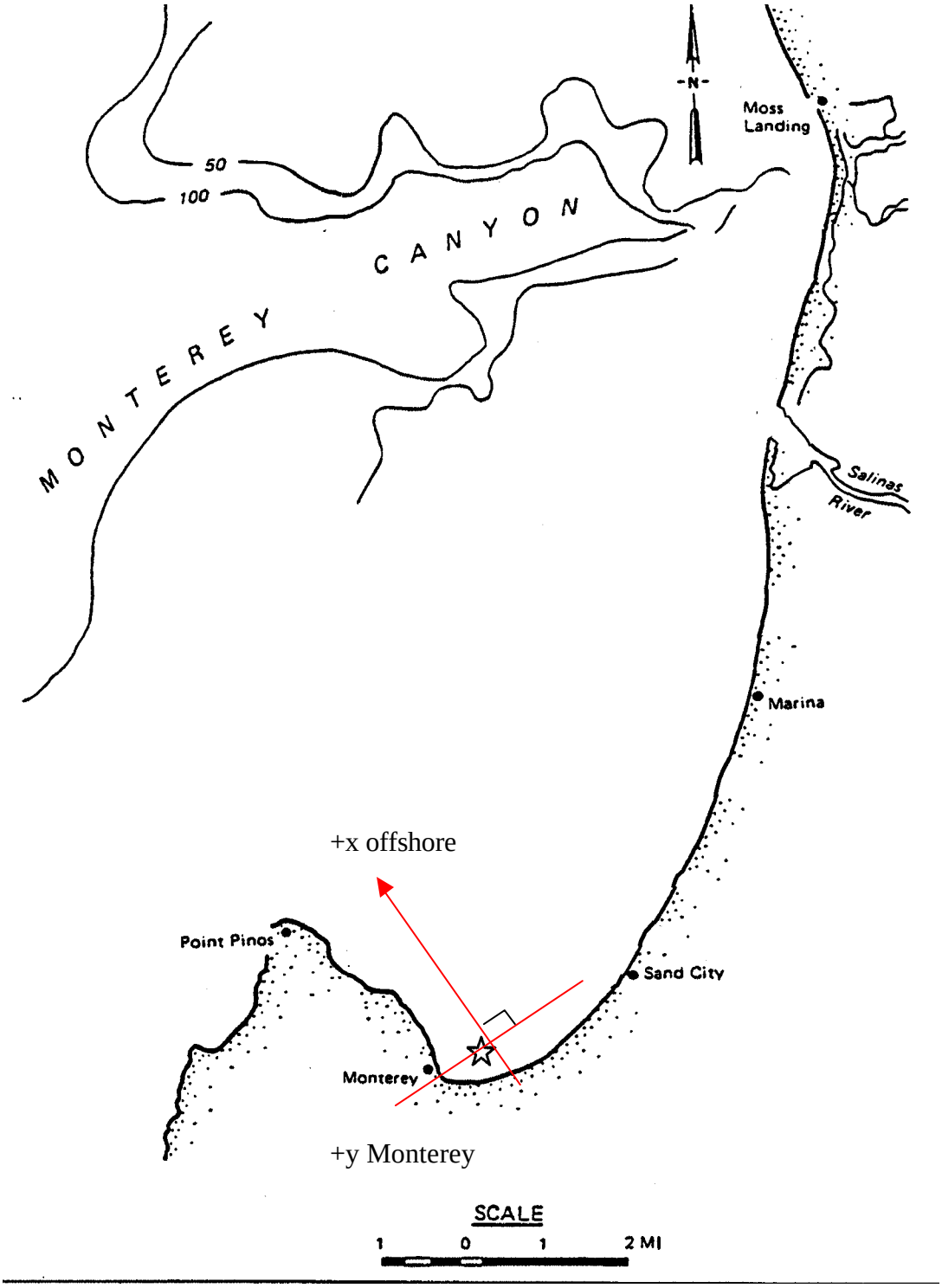

Figure 13. Location of Monterey Bay and the MISO platform off Monterey, CA. The star represents the location of the MISO array. The axis indicates the CS normal coordinate system used in the MISO bottom boundary layer study, with +x offshore, -x onshore and +y south AS and –y north AS.

system by applying a heading rotation to the u and v components to find the CS ($wind_{CS}$) and long-shore ($wind_{LS}$) components.

$$wind_{CS} \cong windspeed(\frac{m}{s}) * \cos[winddirection - 15^{o}(rad) - 180 * (\frac{pi}{180})] \ (ms^{-1}) \tag{5}$$

$$wind_{LS} \cong windspeed(\frac{m}{s}) * \sin[winddirection - 15^{o}(rad) - 180 * (\frac{pi}{180})] \ (ms^{-1}) \tag{6}$$

$$\text{wind rotation} = 360^{o} + (320^{o} - 360^{o}) - 90^{o} \tag{7}$$

B. HEIGHT ABOVE BED REFERENCE

1. CTD

Once the coordinate system was resolved, a fixed vertical depth reference had to be established prior to analyzing any of the field data collected by the CTD and velocity profiling instruments. As the focus of this study is the bottom boundary layer, height above the bed (HAB) reference in meters was selected as vertical coordinate. The pressure-referenced CTD profiles were converted to this vertical reference by using the MISO pressure sensor. The height in meters above the bed of the paroscientific was a known value of 1.2m and the pressure of the paroscientific (p_{paro}) was taken to be the pressure measured by the instrument ($p_{parotatol}$) minus the barometric pressure ($p_{barometric}$)

$$p_{paro} = p_{parototal} - p_{barometric} \quad \text{(dbar)} \tag{8}$$

Using the hydrostatic equation and converting the 5 minute pressure averages from dbar to Pa, the height above the paroscientific (z_{paro}) was then calculated.

$$p = r(\frac{kg}{m^3})g(\frac{m}{s})z(m) \quad \text{(dbar)} \tag{9}$$

$$z_{paro} = p_{paro} * \frac{10^4}{rg} \quad \text{(m)} \tag{10}$$

The distance below the surface (z_η) to the CTD was then calculated in the same manner.

$$z_h = \frac{\lfloor (p_{CTD} - p_{barometric}) * 10^4 \rfloor}{rg} \quad \text{(m)} \tag{11}$$

The height above the bed in meters of the CTD (z_{CTD}) was then found using the variables calculated above.

$$z_{CTD} = 1.2m + z_{paro} - z_h \quad \text{(m)} \tag{12}$$

2. ADCP

The ADCP was adjusted to the HAB reference by first determining the height offset of the ADCP instrument (1.2m), the thickness of the frame (0.03m), and the distance to the first bin (1.61m). By adding each of these components, the HAB of the ADCP was approximated to be 3.19m.

3. BCDV

Before the HAB for the BCDV could be determined, the range to the time-varying bed had to be determined using 30 second backscatter energy. The power of the backscatter was computed. The first maximum power above a given threshold was selected to be the location of the bed. A threshold of $1e^5$ (in arbitrary units) had to be set in order to avoid initial high intensity returns in bubbly conditions. This threshold also

extended to the mid ranges of 50cm to 70cm from the instrument where values greater than $1e^5$ were sometimes encountered due to a large amount of backscatter from suspended sediment. When the threshold was exceeded in this range, the maximum of each power computed was determined to be the range to the bed. Ranges to the bottom bed bin varied anywhere from 79cm to 81cm over the 2 month observation period. This range was then inverted to obtain the HAB for the backscatter and velocity profile timeseries.

THIS PAGE INTENTIONALLY LEFT BLANK

IV. RESULTS

A. SOLITON OBSERVATIONS

Internal tidal bores (ITBs) and solitons were observed regularly at the MISO site during the two-month experiment. The tidal bores propagated both in a cross-shore (CS) and alongshore (AS) direction and contained either single soliton events or packets of solitons on the leading edge. These events had a significant impact on the water column structure as they passed through the observation site. In the following sections, several case studies were chosen to demonstrate and compare the different properties of the CS and AS bITBs and their effect on the water column and the bottom boundary layer.

1. YD 228-228.15

The internal tide of YD 228-228.15 was a clear example of a soliton that formed on the steepening edge of the ITB. Temperature profile timeseries in Figure 14a show strong stratification present at the MISO site with the thermocline at 8-10m HAB before the arrival of the soliton. 4m isotherm displacements down to 6m HAB occur, causing the displaced water to have temperatures 4^{o}C warmer than the background at depth. This large displacement and the opposed top layer and bottom layer current in Figure 14b and 14c indicate that both the soliton and tidal bore are strong mode 1 baroclinic processes. The single soliton on the steep edge of the internal bore arrives at the observation site at YD 228.08 as seen in Figure 14a and 14b. The duration from start to finish of the soliton pulse is approximately 10min and can be considered as a sharp temporal version of the internal tidal bore which has a duration from the leading edge to maximum amplitude of approximately 75min.

Both the ITB and solitons of YD 228 are highly nonlinear baroclinic processes in which isotherm displacements and velocities change suddenly with depth and time as pulses, rather than sinusoidal oscillations. Temperature profile timeseries show a strong near surface stratification present prior to the arrival of the soliton and ITB. As the ITB pass in these very shallow conditions, the stratification changes rapidly from near surface to near bed. Current vector profiles every 1m from 3m to 12m HAB also show a very rapid change in currents as they switch sign during the passage of the ITB and soliton in

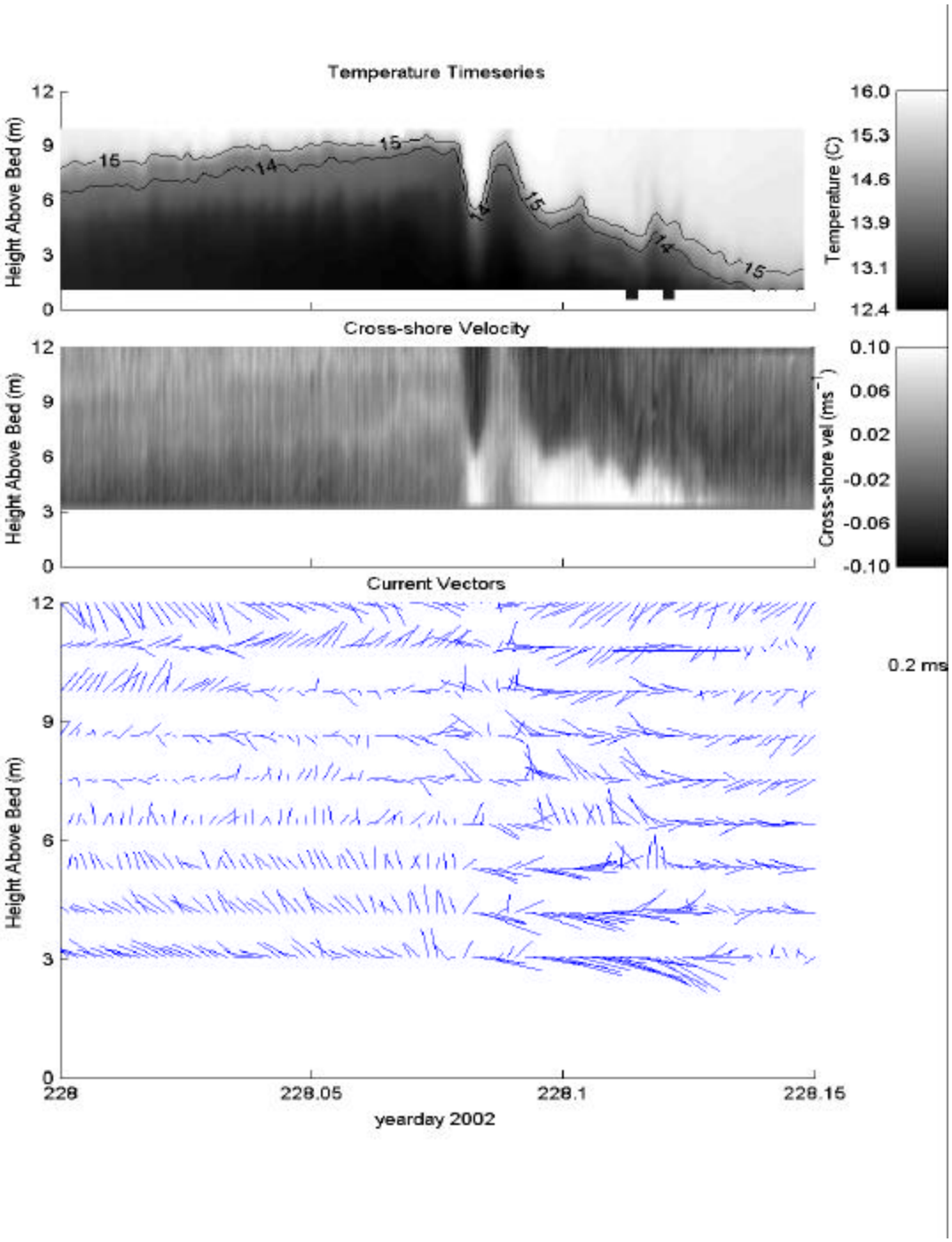

Figure 14. Yearday 228-228.15. (a) Temperature profile timeseries. (b) ADCP CS velocity profile timeseries. (c) Current vectors. Vertical alignment of isotherm and current displacement are indication of a soliton and internal tidal bore.

Figure 14c. Both the ITB and soliton have velocity signatures of $0.10 ms^{-1}$ predominantly onshore near the surface, indicating that the bore is propagating CS from the shelf break directly offshore of the MISO site. Due to the baroclinicity of the approximately two-layer system, currents below the bore and soliton are moving with comparable velocities of $0.10 ms^{-1}$ but in the opposite direction (onshore). The current vectors illustrate how the water column is weakly sheared prior to the onset of the bore, with steady currents of $0.02\text{-}0.05 ms^{-1}$ moving in a +AS direction near the surface and the bed and with no sudden changes occurring from YD 228-228.08. As the soliton approaches the observation site, the currents become increasingly offshore from 12m to 8m HAB at YD 228.08, but continue to stay rather AS from 7m down to the bed. However, during the passage of the soliton and ITB from YD 228.08-228.15, currents at 10m HAB rotate to an onshore direction. Within the ITB and soliton, current velocities rotate 180^{o} indicating water being pushed onshore (-x) direction, while below the soltion and the leading edge of the ITB waters are being pulled offshore with the same magnitude. These sudden, pulse-like currents associated with solitary internal waves and internal tidal bores have significant effects on the water column as they are the dominant currents occurring at the site.

2. YD 229-229.1

The packet of solitons occurring during YD 229-229.1 is an example of multiple solitons that have formed on the leading edge of an ITB. Temperature profile timeseries in Figure 15a shows strong stratification present similar in structure to YD 228, with the thermocline at 8-10m HAB prior to the arrival of the bore. Again, approximate 4m isotherm displacements occur. These large isotherm displacements and opposed top layer and bottom layer current in Figure 15b and c, again show the strong mode 1 baroclinic processes controlling these currents.

Unlike the soliton and ITB found in YD 228-228.15, these 3 packet solitons and their ITB are not as steep, but rather weaker and broader, and have decreasing, rank ordered amplitude. The duration of these packet solitons are on the order of 15min, approximately 1/3 longer than the sharp pulse soliton in YD 228. As in YD 228, isotherm displacements and velocities change suddenly with time and depth and occur as pulses rather than sinusoidal oscillations. Within the temperature profile timeseries of

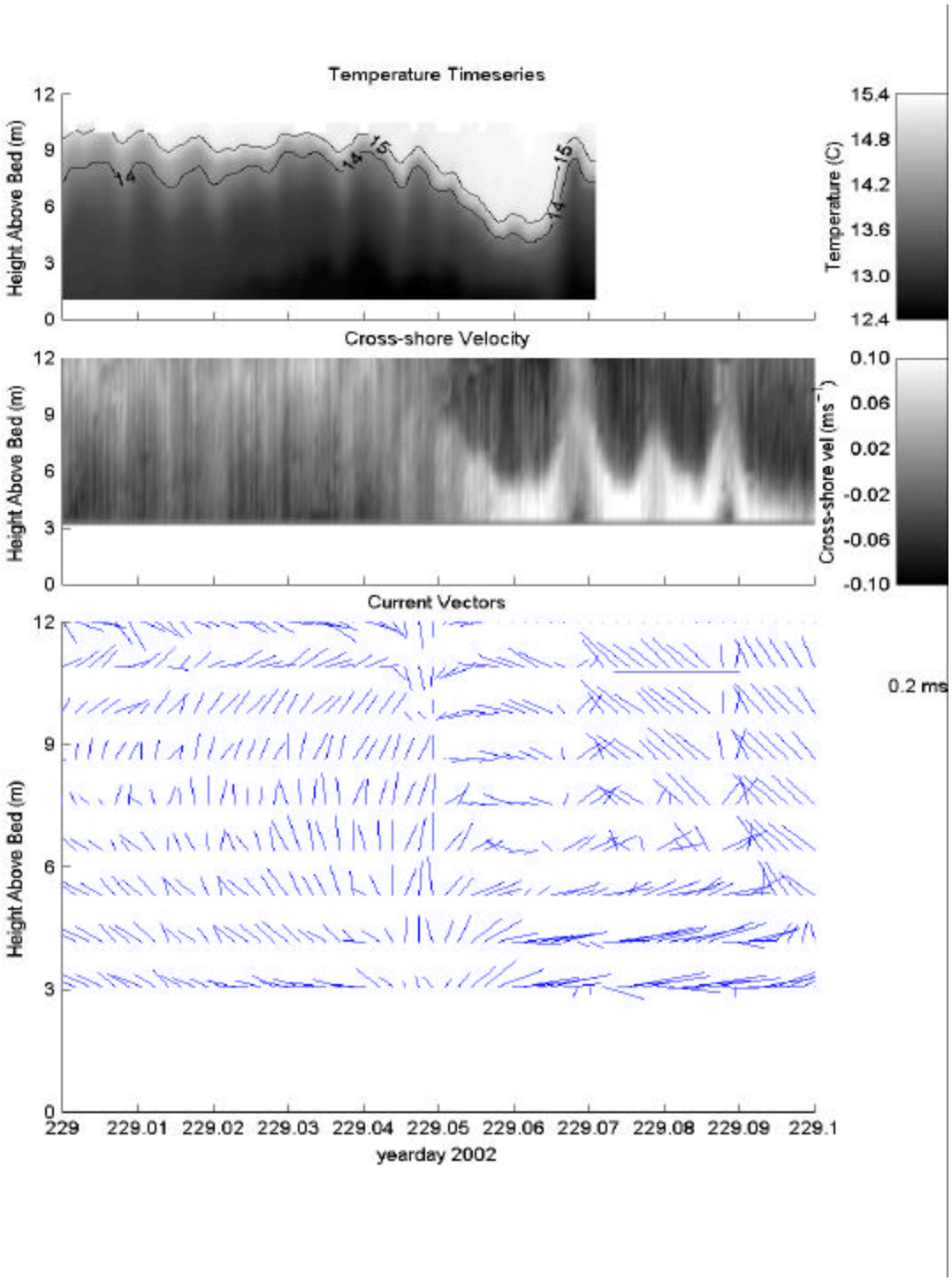

Figure 15. YD 229-229.1 (a) Temperature profile timeseries. (b) CS ADCP current velocity profile timeseries. (c) Current vector timeseries. CS ADCP current velocities indicate solitons as part of a wave train.

Figure 15a, strong, near surface stratification is present prior to the arrival of the ITB and packet solitons and changes rapidly to near bed as they pass in the shallow conditions. Current vector profiles every 1m from 3m to 12m HAB show a weaker change down through the water column as the packet solitons move through from YD 229.05-229.1. However, the CS signatures have approximately the same magnitude as in YD 228 with predominately onshore currents of $0.10 ms^{-1}$ near the surface and offshore currents of comparable velocities below the solitons. As in YD 228, the current vectors in Figure 15c for YD 229 illustrate a stable water column prior to the arrival of the solitons with currents of $0.05 ms^{-1}$ in a +AS direction from YD 229-229.05. However, during the arrival and passage of the first soliton at YD 229.05, currents from 6-10m HAB rotate to an onshore direction. This onshore current decreases in magnitude and becomes more +AS as each successive soliton arrives at the observation site. The current vectors indicate that within each soliton, water is being pushed onshore, becoming more +AS through the packet, while below the soliton, waters are continuously being pulled offshore with equal or greater magnitudes. The soliton packet of YD 229 are sudden pulse-like currents, but of longer duration and weaker magnitude compared to YD 228 events, with similar effects on the water column.

B. INTERNAL TIDE BORE (ITB) OBSERVATIONS

By expanding the timeseries to a 24-hour period, the effects of the semidiurnal ITB over two cycles can be seen more clearly in YDS 228, 229, and 232 in Figures 16, 17, and 18, respectively. These three one day timeseries illustrate ITBs with decreasing steepness, and consequently fewer solitary internal waves (SIWs), over a four day interval.

1. YD 228

The steep edge of the ITB is clearly seen in YD 228 in the temperature and CS velocity profile timeseries of Figure 16a and 16b. Because of missing temperature data, the semidiurnal nature of the bore is not seen in the temperature profile timeseries, but the stronger first bore can be seen in the CS velocity profile. The first ITB that occurs at YD 228.1 is much steeper and stronger than the second ITB occurring later on that day as seen in the temperature and CS profile timeseries of Figure 16a and 16b. The steep leading edge of this first dominant bore enables nonlinearites to develop and form the

sharp soliton pulse seen in the previous case study of YD 228-228.15 in Figure 14. The steep edge duration of this ITB is on the order of 75min, while the weaker second bore is difficult to define. However, both of these tidal bores have a nominal periodicity of 12 hours. These top and bottom layer opposed currents are not as dominant for the weaker and less steep second bore.

A fourth order low pass Butterworth filter with a cutoff of 5min was used to filter out higher frequency solitary internal wave events in order to focus on the effects of the ITB on currents throughout the depth of the water column in Figure 16c. Low passed filtered current vectors indicate that just prior to the arrival of the ITB from YD 228-228.08, currents of $0.01ms^{-1}$-$0.05ms^{-1}$ are present in the +AS direction. However, upon the arrival of the ITB at YD 228.08, near bed currents rotate onshore with speeds of 0.02-$0.05ms^{-1}$ within the steep leading edge and offshore with equal magnitude just below it. As the tidal bore passes the observation site, baroclinic processes push water onshore from the surface down to 6m HAB and offshore from 6m HAB to the bottom during the duration of the bore from YD 228.08-228.15. At the maximum amplitude displacement of the ITB (YD 228.15), currents return to a depth dependent + or – AS direction. Because the second bore arriving at YD 228.6 is not as steep and much weaker than the first bore, no onshore movement of water is observed within the leading edge, however, a slight offshore current is seen directly below it from 5m-3m HAB at YD 228.7. +AS currents are more prevalent in this weaker bore, possibly indicating that it was not generated directly offshore at the shelf break, but rather at the Monterey Canyon and has propagated down the bay.

2. YD 229

YD 229 is another example very similar to that of YD 228. Again, two ITBs are readily observed in the temperature profile timeseries of Figure 17a, with the first one being much steeper, with displacements of 8m and currents $>0.1ms^{-1}$. The first ITB arrived at the observation site at YD 229.08 and contains the packet of solitons that was discussed in case study 229-229.1. Like the solitons, this bore is not as steep as the first bore that occurred during YD 228. The steep edge duration of this first bore is approximately 3.5 hours long, which is more than twice as long as the previous example.

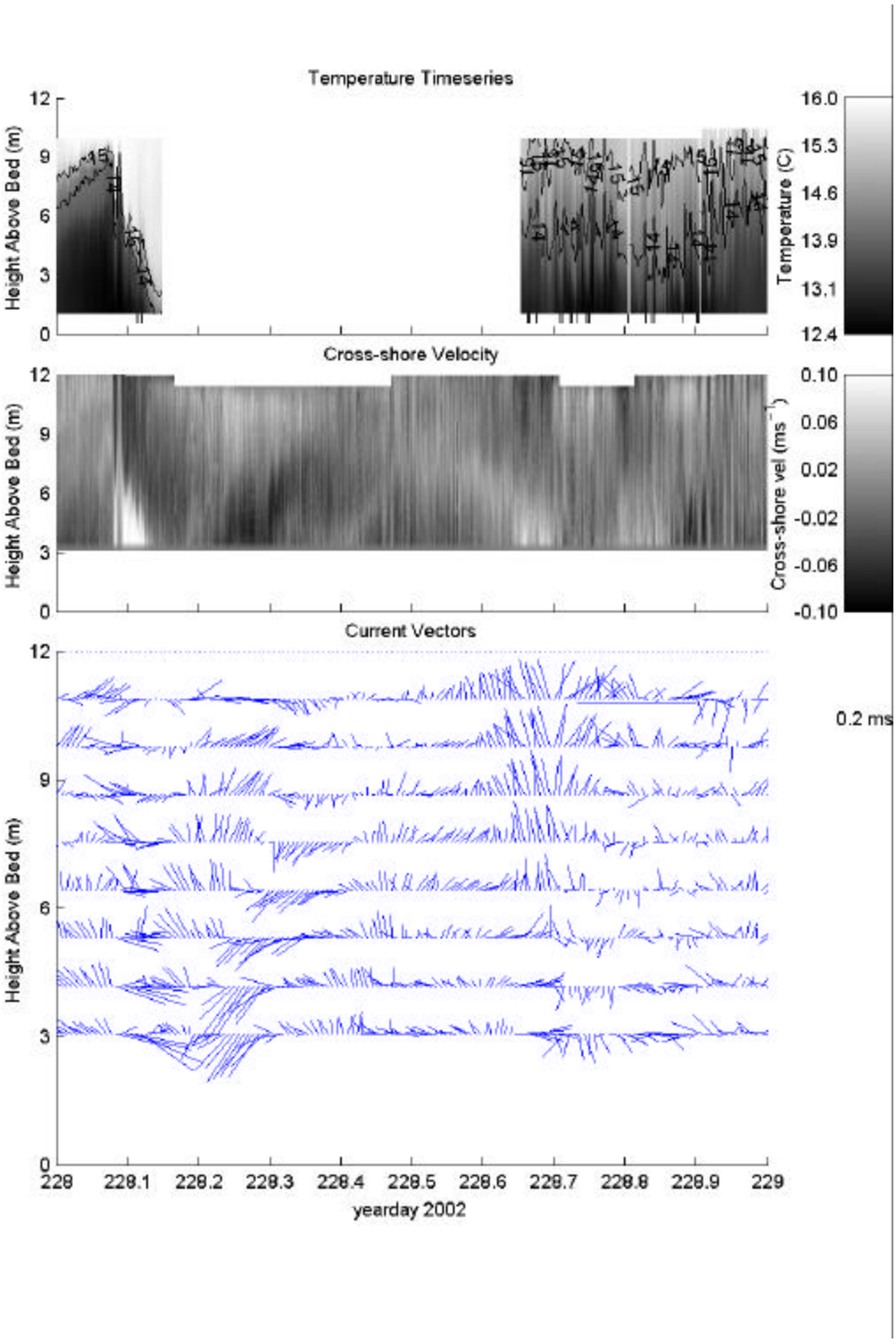

Figure 16. YD 228-229. (a) Temperature profile timeseries. (b) CS ADCP velocity profile timeseries (c) Low pass filtered current vectors. Although the temperature timeseries has missing data, the semidiurnal internal tidal bore is evident in the CS ADCP velocity and current vector timeseries.

The second bore occurs at YD 229.75 and is not as clearly defined in the temperature profile timeseries or the velocity profile timeseries, making it difficult to approximate its steep edge duration.

By examining both the temperature and velocity profile timeseries (Figures 17a and 17b), the first ITB has large isotherm displacements down to 2m HAB and rapid velocity changes with depth and time. Stratification again changes from near surface to near bed during the passage of this ITB and CS velocities are observed to be onshore within the leading edge and offshore just below it. In contrast, the second ITB has very small isotherm displacements of 4m, and no significant changes in the CS velocities. Stratification is seen to change only slightly and remains predominantly near surface, while no sudden changes in CS velocities are observed between the leading edge and the currents below it.

Figure 17c shows the low passed filtered current vectors for YD 229. Prior to the arrival of the first ITB and its soliton packet, current are $0.05 ms^{-1}$ in the +AS direction. As the soliton packet arrives at YD 229.08, currents from 12m down to 7m HAB rotate slightly to an onshore direction, but with a strong +AS component, while the currents directly below the solitons, nearer the bed from 5m-3m HAB, rotate to an offshore direction. In contrast, currents near the peak displacement of the ITB rotate back to a +AS direction, but remain offshore beneath it. After the maximum amplitude displacement of the ITB, currents reverse to a –AS direction throughout the depth of the water column. The strong AS currents that occur in conjunction with the CS currents indicate that the ITB has strong vortical mode. The second ITB, in contrast, has no significant impact on the currents within the water column as they remain fairly +AS throughout its passage. However, a small offshore current is observed under the broad, weak leading edge of the bore from 7m-3m HAB at YD 228.85. Once the maximum amplitude displacement occurs at YD 229.9, currents return to a +AS direction, in contrast to the –AS direction of the first ITB.

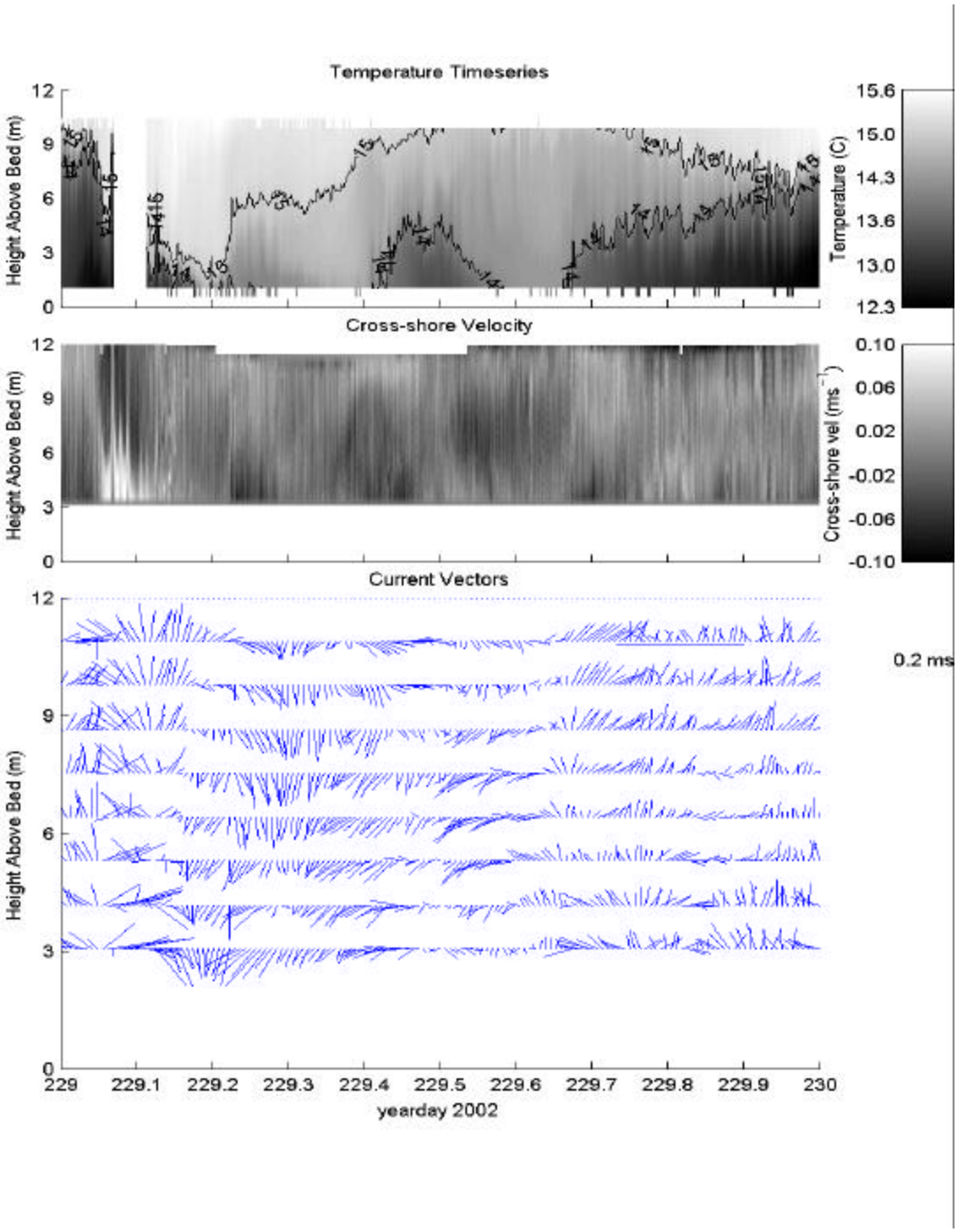

Figure 17. YD 229-230(a) Temperature profile timeseries. (b) CS ADCP velocity profile timeseries (c) Low pass filtered current vectors. Although the temperature timeseries has missing data, the semidiurnal internal tidal bore is evident in the CS ADCP velocity and vector timeseries.

3. YD 232

YD 232 had a contrasting example of two low slope ITBs (Figures 18a and 18b). The first bore occurring at YD 232.2 has decreased in steepness when compared to the ITBs of YD 228 and 229. The broad, leading edge of this bore is not capable of generating any distinct or dominant solitons as in the previous two cases. The second bore observed at YD 232.75, like the first, has a broad leading edge that has not generated any solitons. However, both of the ITBs occurred with equal magnitude, unlike the previous cases where the first bore was significantly dominant over the second one. The semidiurnal nature of these two bores is in the CS profile velocity timeseries with a period of 12 hours. The steep edge duration of these two ITBs is approximately 4 hours long, more than twice as long as the steeper edge bores of YDS 228 and 229.

Mode 1 baroclinic processes are again evident for this case with isotherm displacements down to 3m HAB occuring on the leading edge of the two ITBs. During the passage of each bore, stratification changes from near surface to near bed as was observed in the previous two examples. Changes in CS velocity between the upper and lower layers are observed as well, but are much weaker when compared to the steeper edge bores of YDS 228 and 229.

Currents prior to the arrival of each bore are in a +AS direction (Figure 18c). A strong vortical mode is present in the currents upon the arrival of the first ITB as currents are transitioning from +AS to –AS seen from YD 232.0-232.3. Within this time period, currents from 12m-5m HAB rotate rapidly from +AS to onshore to –AS. These onshore currents are occurring within the leading edge of the ITB. However, just below the leading edge of the bore from 5m-3m HAB, currents rotate rapidly from +AS to offshore to –AS. Like YD 229, the second bore remains fairly +AS through its passage from YD 232.6-232.9 with a slight offshore current directly beneath the leading edge from 7m-3m HAB occurring at YD 232.8, indicating a weaker, but present vortical mode. Because this bore is propagating in a +AS direction, it was most likely generated at the axis of the Monterey Canyon to the north of the observation site and was refracted down the bay.

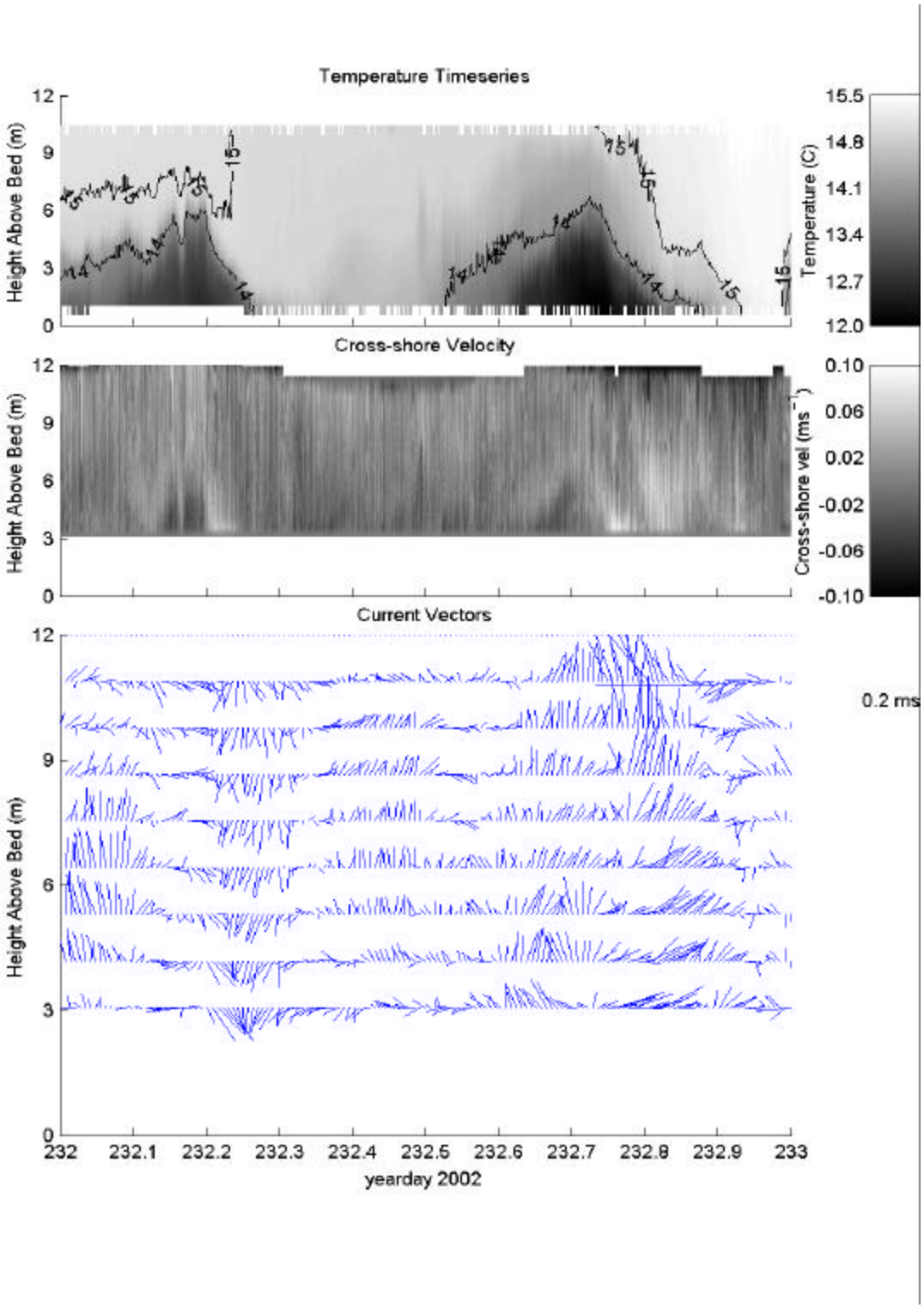

Figure 18. YD 232-233. (a) Temperature profile timeseries (b) CS ADCP velocity profile timeseries shows clear indication of the semidiurnal internal tidal bore. (c) Low pass filtered CS vectors illustrate the baroclinicity of the water column.

The second bores of YDS 228, 229 and 232 are clear examples of bores that were not generated at the shelf break directly offshore, but more likely at the Monterey Canyon then subsequently refracted to propagate AS down the bay. Because these bores traveled a greater distance to reach the observation site is a possible indication that energy was lost due to dissipation as was indicated by their broader leading edges and weaker CS velocity signatures. Unlike the first ITBs of YDS 228 and 229, there were no dominant soliton events on the leading edge of these secondary bores. The energy loss most likely prevented solitons from evolving or caused them to decay before reaching the observation site.

The above case studies indicate that tidal bores moved regularly in both the CS and AS direction. The bores generated at the shelf break directly offshore of MISO propagated in a CS direction and were observed to contain single or multiple soliton depending on the steepness of the leading edge. These events were capable of pushing currents onshore near the surface and offshore near the bed. However, the bores generated at the axis of the Monterey Canyon to the north of MISO, propagated in an AS direction and were much broader and weaker and therefore, contained no solitons on the leading edge.

4. Tidal Cycle

The ITBs observed over the four-day period from YDS 228-232 are not closely tied to the barotropic tidal cycle. The ITBs pass through the observation site at different times each day. The first ITB of YD 228 occurs near the spring tide of the semidiurnal barotropic tide (Figure 19). The bore happens to pass through the observation site during the ebb cycle of the first high tide, at a time determined by the propagation delay between the generation and observation sites (Figure 20). This bore was generated during the transition from ebb to flood flow of the previous 2nd high tide (YD 227). However, the second, weaker bore passes through the observation site during the ebb cycle of the second high tide and was generated at the shelf break during the transition from ebb to flow of the previous first high tide (YD 228). This same pattern is observed for the ITBs of YDS 229 and 232 in Figure 20, where the steeper first bore (large star) passes the

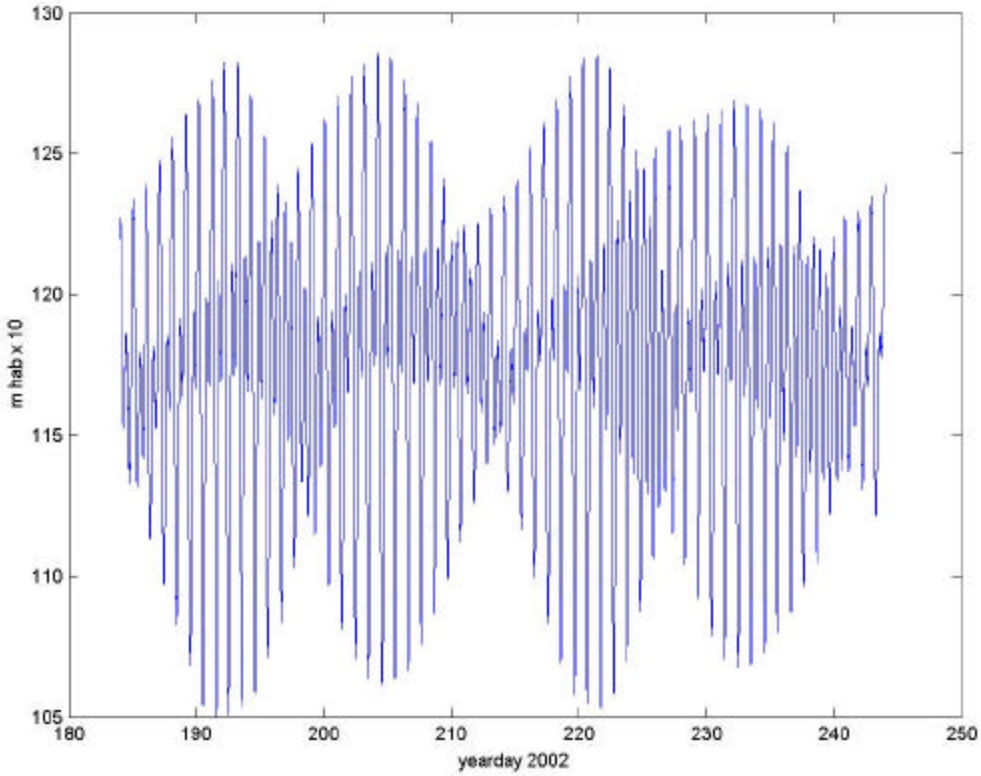

Figure 19. Tidal timeseries from YD 184-244. Periods of maximum amplitude are known as spring tides and period of minimum amplitude are neap tides. YD 228 is occurring near the spring tide of the tidal cycle.

observation site during the ebb cycle of the first high tide, being generated within the second high tide of the previous day, while the second weaker bore (small star) passes during the ebb cycle of the second high tide, being generated within the first high tide of that day. The amplitude displacement that occurs between max flood and max ebb for the second high tide is 5m which is much smaller than the 20m displacement for the first high tide. Less energy is lost for the smaller displacement allowing the bores generated from it to be the stonger and steeper. However, because more energy is lost for larger displacements, the ITBs generated from it tend to be weaker and broader. The ITBs are also assisted by the respective tide that carries them through the observation site. The strong ITBs pass through MISO during the larger magnitude first high tide, while the weak ITBs pass through during the lower magnitude second high tide.

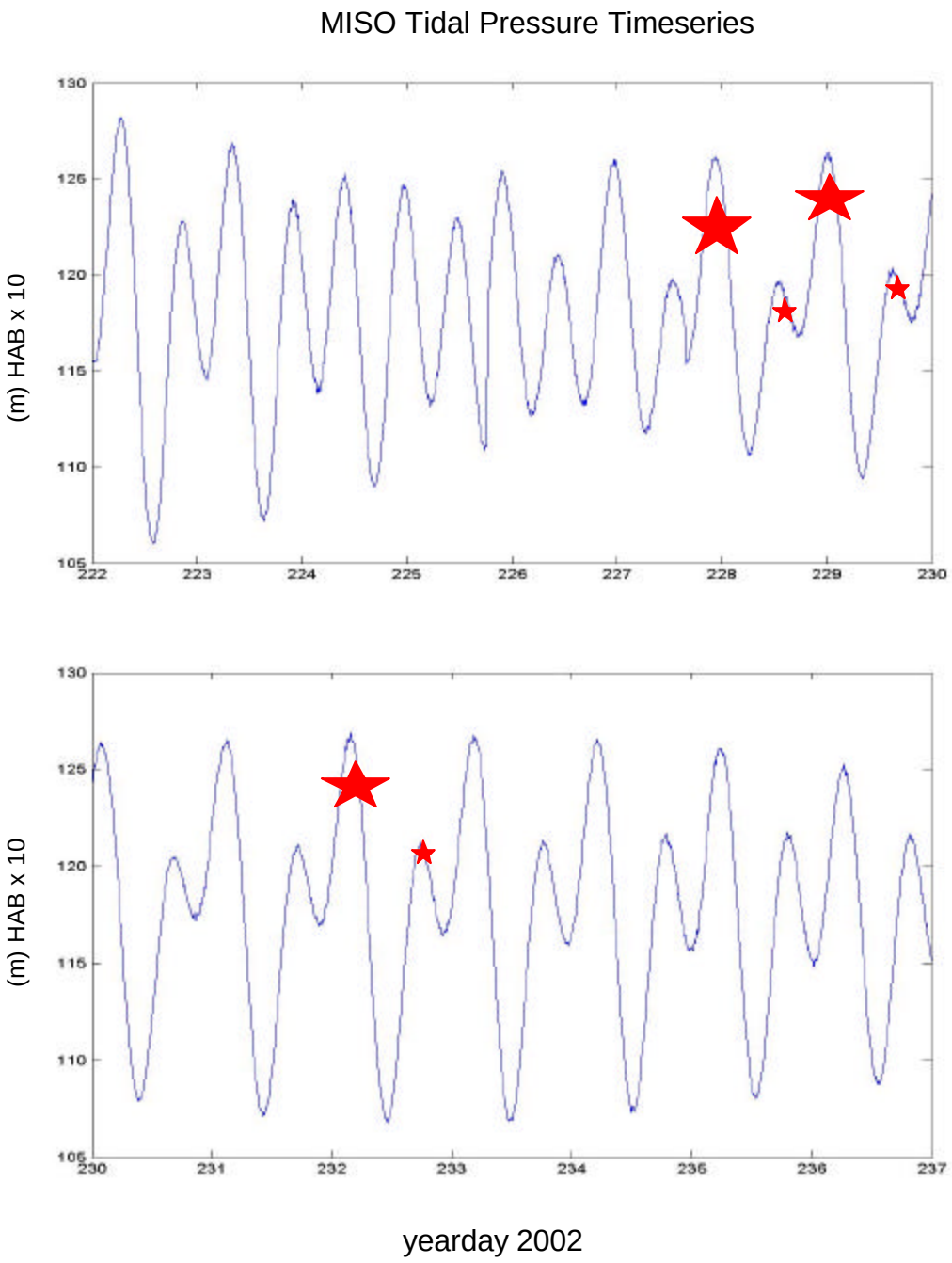

Figure 20. Tidal Pressure Timeseries showing the four day period between YDS 228-232. Vertical axis is in m (HAB) x 10. ITBs are indicated in the figure as stars. The steeper first ITBs (large stars) that were observed at MISO occurred during the ebb flow of the first high tide, while the weaker second ITBs (small stars) occurred during the ebb flow of the second high tide.

C. BOTTOM BOUNDARY LAYER OBSERVATIONS

The internal tidal bores and accompanying solitons at the MISO site produced currents near the bed significantly greater than background levels. The pulses of current generated a deep boundary layer above the bed, and it is of interest to see whether these currents contributed significantly to sediment suspension. The evolution of a logarithmic layer was observed as the ITB and soliton currents moved over the sandy, mobile bed. This resulted in a wall bounded shear flow. By using the "Law of the Wall" in the region far from the viscous sublayer, a dimensional analysis yields (Kundu 1990)

$$\frac{dU}{dz} = \frac{u_*}{kz} \tag{13}$$

Integration gives

$$U(z) = \frac{u_*}{k}\ln(z) + const. \tag{14}$$

A profile plot using log(z) versus current speed, reveals a logarithmic layer as a straight line. In this region, U (current speed) is related to u_* by the equation

$$U(z) = \frac{u_*}{k}\ln(\frac{z}{z_o}) \tag{15}$$

and so

$$u_* = \frac{U(z)k}{\ln(z)} \tag{16}$$

where $\frac{U(z)}{\ln(z)}$ is the inverse slope of the logarithmic layer, and k is the Von Karman constant, approximately 0.41. Values of u_* under the SIWs and ITBs were on the order of 0.01-0.03ms^{-1} as ITBs passed the MISO site. These high friction velocity values indicate that significant stress occurs due to friction drag as the SIW flow field interacts with the dynamically rough bed. Because u_* values scale roughly with the mean current, as the mean current approaches zero, so does u_*, and the friction velocity becomes difficult to estimate from fits to the log profiles. Once the friction velocity has been estimated, the shear stress above the bed is then estimated from

$$t = \rho u_*^2 \quad (17)$$

where ρ is the density of the water.

Very near the bed layer (0mm) in the viscous sub-layer, molecular viscosity effects dominate fluid movement. This region is too small a scale to be studied in our bottom boundary analysis. In coastal areas with sandy beds, ripples have been observed to dominate the apparent roughness over mobile, sandy beds. Since surface gravity waves result in oscillatory fluid motion down to the bed, a thin wave boundary layer forms, which tends to decouple fluid movement from above. This occurs when there are significant levels of long period surface gravity wave energy within the water column. This wave boundary layer causes the mean currents to attenuate very slowly above the bed in the log layer (Figure 21). Without the presence of this wave boundary layer, the logarithmic layer has a direct interception to zero current (Figure 22).

A logarithmic layer evolves above the bed as the baroclinic flows from SIWs and ITBs pass the MISO site. This turbulent shear layer is bounded above by strong stratification associated with baroclinic events. Because this analysis focuses on the effects of solitons on the bottom boundary layer, stress timeseries are estimated from the near-bed logarithmic layer. Within the logarithmic layer, there is an inertial transfer from the viscous sublayer to the wave boundary layer and then the logarithmic outer layer by inviscid nonlinear processes.

Polynomial fitting and regression techniques have been used to automatically determine the slope of this logarithmic layer to produce timeseries of u_*. Between 4cm above the bed to 7cm, a linear regression line was calculated and its regression coefficient was found. Points were added one cm at a time until the correlation began to decrease. The fit that scored the highest correlation value above 0.80 was used to determine the slope of the logarithmic layer (Figure 23). This slope was then used to find the zero velocity intercept, giving a coarse estimate of the apparent roughness of the bed. These values of Z_o were only resolved to 1cm, but provided Z_o estimates for high roughness conditions. With steady flow over the bed, a wake is generated behind each bump in the bed and stress is transmitted to the bed by way of a pressure drag on the roughness elements.

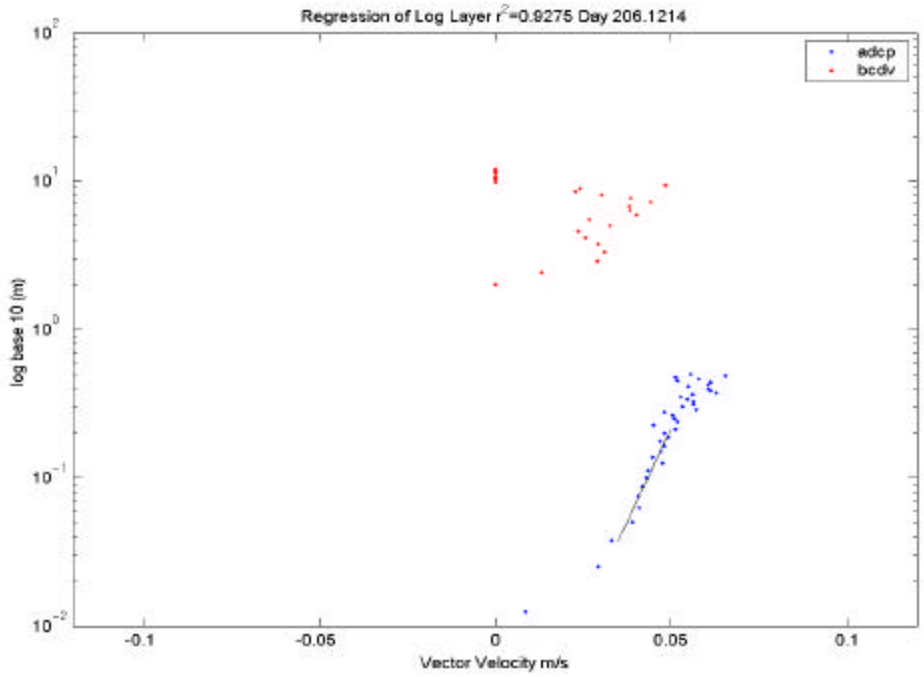

Figure 21. A plot of total velocity with $\log_{10}(z)$ vertical coordinate for a 30sec mean current. Slow attenuation of the logarithmic layer for YD 206.12, during a high energy wave day caused by the wave boundary layer.

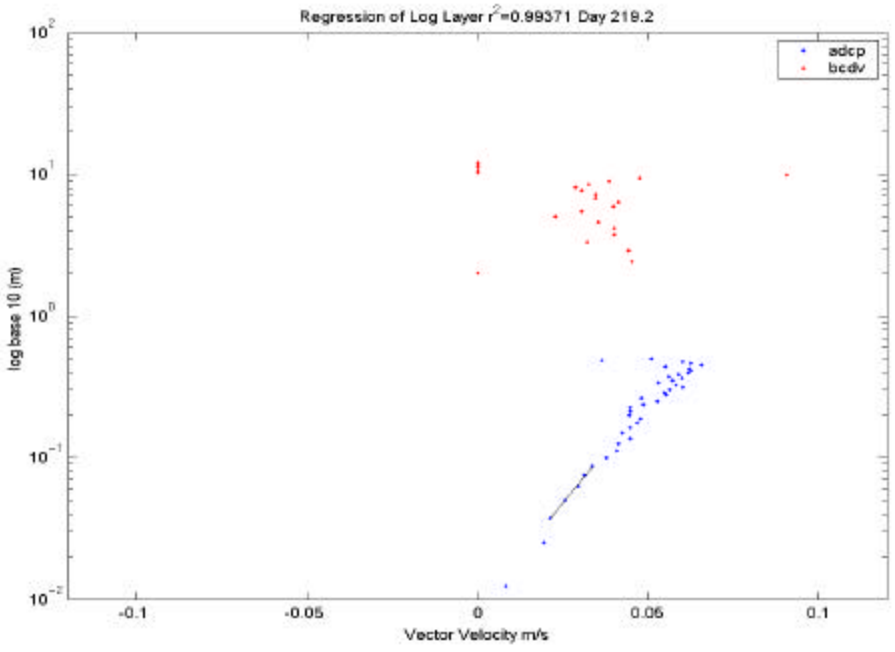

Figure 22. A plot of total velocity with $\log_{10}(z)$ vertical coordinate for a 30sec mean current. Fast attenuation of the logarithmic layer for YD 219.2, during a low energy wave day caused by the absence of the wave boundary layer.

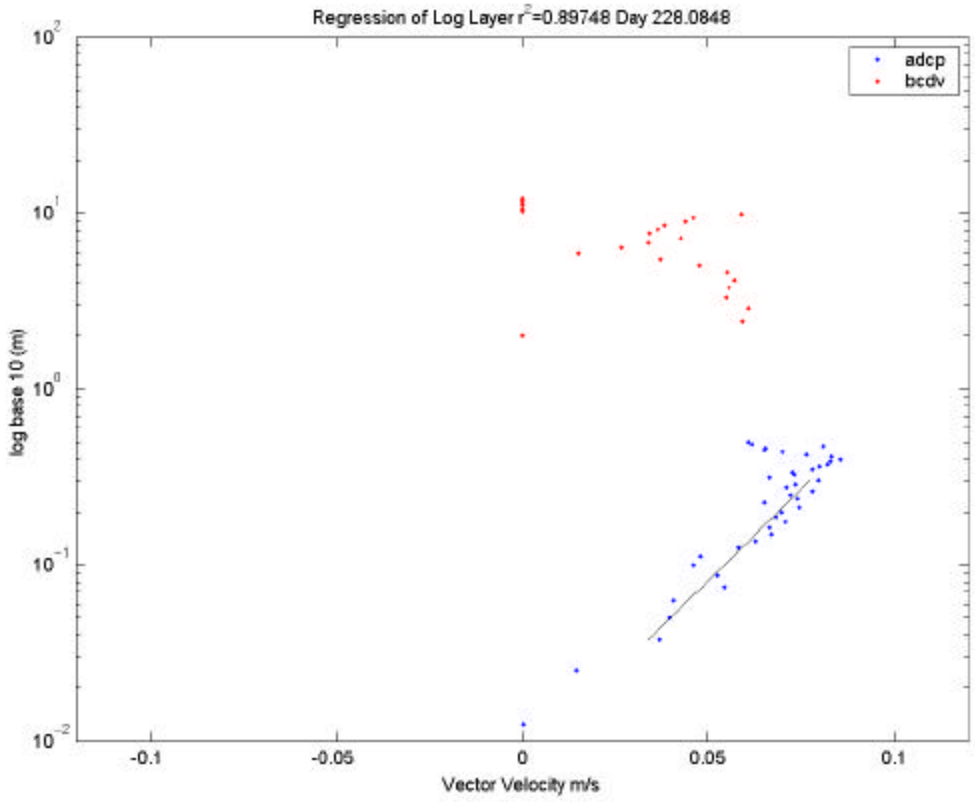

Figure 23. Linear regression of the logarithmic layer for YD 228.08 and calculation of the slope.

The effects of SIWs, ITBs, and surface gravity waves on the bottom boundary layer and sediment suspension are considered over a range of forcing conditions in Figures 24-29. In each of these 3-hour timeseries, broken into two groups of high and low surface gravity wave energy days, the RMS wave velocity at 3m HAB, 3m HAB mean ADCP and 4-18cm HAB mean BCDV current components, Shields Parameter (Chapter V), relative backscatter profiles (that scale with sediment concentration), and friction velocity are shown.

1. High Wave Energy

Relatively high wave energy days are shown in Figures 24, 25 and 26 for YDS 200.8, 206.05, and 219.05. YD 200.8 shown in Figure 24 was one of the first high wave energy days encountered during the two month observation period. During this 3-hour period RMS wave velocities were approximately 0.12ms^{-1} as seen in Figure 24a. Effects

of this high wave energy, due primarily to surface gravity wave swell, is seen in the backscatter profile where shades of white indicate high backscatter and shades of gray and black indicate areas of low backscatter (Figure 24d). These backscatter values scale with sediment concentration. The increase in backscatter from black to white values corresponds to sediment concentrations that have increased by 3 orders of magnitude. Figure 24b shows the 3m HAB mean ADCP (bold line) and 4-18cm mean BCDV CS velocities. A sharp soliton pulse in the lower 40cm with an onshore velocity of $0.10 ms^{-1}$ is observed at YD 200.92 on the leading edge of an ITB with a CS velocity of the same magnitude. The presence of the strong swell wave boundary layer has also helped to decouple the fluid from above resulting in a small vertical velocity gradient from 3m HAB down to the lower 40cm.

The instantaneous Shields Parameter (q'), which is an indication of when sediment motion is initiated (to be discussed further in Chapter V), is shown in Figure 24c. After a sensitivity analysis, twice Jonsonn's (1967) wave friction factor was used to illustrate the effect of high surface gravity wave forcing. The critical Shields Number (q_{crit}) for the well-sorted sediment at the site is 0.05, and is a rough indicator of when sediment suspension will occur. Prior to the arrival of the soliton and ITB at the observation site, q' has a value of 0.06-0.08, indicating that the surface gravity wave forcing is strong enough to suspend sediment past q_{crit}. However, during the arrival and passage of the soliton and ITB, q' increases significantly to values of 0.06-0.12, well above q_{crit} and the values that were generated by the surface gravity waves, indicating that the soliton and ITB coupled with surface gravity wave forcing provided more than enough stress to suspend sediment. It is evident, therefore, that the stress generated by high surface gravity wave forcing results in wave-dominated friction velocity values of $1.5\text{-}2.0 cms^{-1}$ from YD 200.8-200.9 in Figure 24e. The friction velocity is seen to increase significantly when a SIW and ITB arrive with strong near bed currents. The bold line indicates the critical friction velocity of $1.51 cms^{-1}$ (to be discussed further in Chapter V), in which values exceeding this will cause sediment suspension. The high suspended sediment profiles (Figure 24d) show the surface gravity wave forcing to be sufficient to produce a large suspended load.

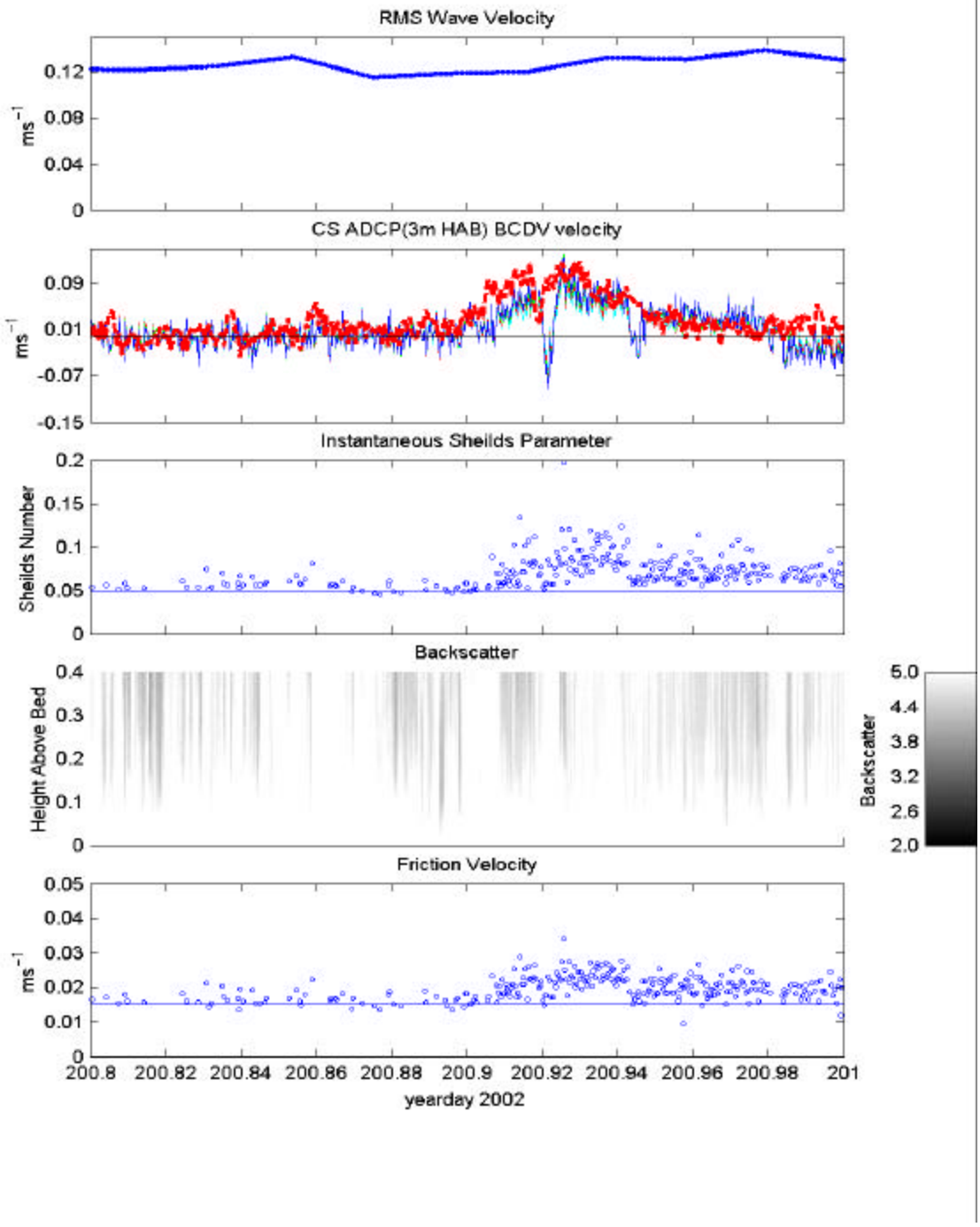

Figure 24. YD 200.8-201. (a) RMS Wave Velocity (b) CS ADCP (3m HAB) (bold line) and BCDV (4-18cm HAB) (c) Instantaneous Shields Parameter q_{crit}=0.05 is denoted by the threshold line (d) Backscatter profile timeseries (e) Friction Velocity u* u_{*crit}=1.51cms^{-1} is denoted by the threshold line.

YD 206.05-206.2 in Figure 25 is a moderate surface gravity wave energy day with RMS wave velocities of 0.07ms^{-1} at 3m HAB (Figure 25a). The backscatter profile timeseries of Figure 25d shows an increase in sediment suspension that occurs when an ITB with multiple solitons passes through the observation site at YD 206.12. Unlike the previous example, where high backscatter was occurring from strong surface gravity wave forcing, the SIW and ITBs contribute significantly to suspension here. In this case, the surface gravity waves are not as strong in causing sediment suspension. Rather it is the ITB and solitons coupled with the moderate surface gravity wave energy that is able to generate suspended sediment. Figure 25b reveals the multiple weak soliton packets, which are both weaker and less steep, than the previous example shown. The peaks of the weak soliton currents at 3m HAB are nearly out of phase near the bed. The effects of these weaker events are evident in the q' and u_* timeseries of Figure 25c and 25e as they only help to slightly increase the values past the critical thresholds. However, the backscatter timeseries does indicate that these events, though weak, when coupled with a moderate surface gravity wave forcing, are capable of suspending sediment in the water column.

YD 219.05 in Figure 26 is another example of a high surface gravity wave energy day, but coupled with a rather weak soliton and ITB. RMS wave velocities shown in Figure 26a are high, exceeding 0.12ms^{-1}. This high surface gravity wave forcing is again evident in the backscatter profile timeseries of Figure 26d, where the lighter areas are approximately 2-3 orders greater in sediment concentration than the darker areas. The highest backscatter occurs at the peak RMS wave velocity of 0.12ms^{-1} at YD 219.07, indicating that surface gravity waves are causing sediment to become suspended above the bed. As the RMS wave velocity slowly decreases within the 3-hour timeseries to 0.08ms^{-1}, high backscatter still occurs. This is assisted by the arrival of solitons and an ITB at YD 219.12. Multiple solitons are observed in the CS ADCP and BCDV velocities of Figure 26b with rather weak near bed velocities of 0.02-0.06ms^{-1}. As in YD 200.8, the wave boundary layer reduces vertical shear in CS velocities between 3cm and 40cm. However, unlike in YD 200.8, these solitons and the ITB appear broader and not as steep and therefore, do not have as significant of an impact on increasing values of q' and u_* as seen in Figure 26c and 26e. These two timeseries do indicate that the strong surface

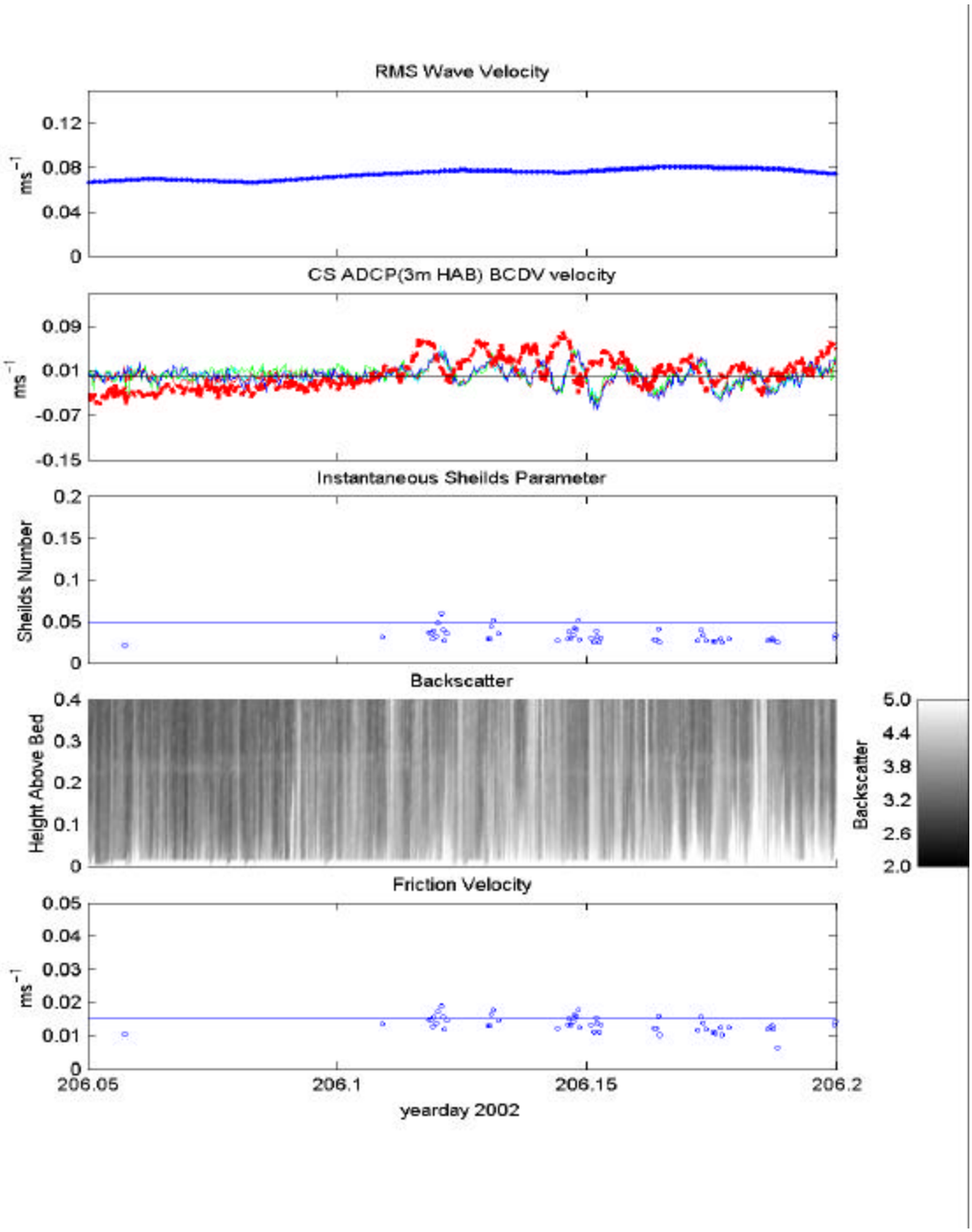

Figure 25. YD 206.05-206.2. (a) RMS Wave Velocity (b) CS ADCP(3m HAB) (bold line) and BCDV (4-18cm HAB) (c) Instantaneous Shields Parameter q_{crit}=0.05 is denoted by the threshold line (d) Backscatter profile timeseries (e) Friction Velocity u* u_{*crit}=1.51cms^{-1} is denoted by the threshold line.

gravity waves are suspending sediment, but that the solitons and ITB help to sustain sediment suspension as the wave energy decreases.

2. Low Wave Energy

YDS 191, 214, and 228 (Figures 27, 28 and 29) are counter examples to those described above. YD 191 is a clear case of low surface gravity wave energy coupled with strong soliton pulses and a steep edge ITB. Here, the low surface gravity wave energy in the water column is reflected in the RMS current velocities of 0.04 ms^{-1} (Figure 27a). Because the wave boundary layer is much thinner and weaker at these low values, CS ADCP and BCDV velocity profiles of Figure 27b indicate a significant vertical velocity gradient in the lower 40cm. The near bed velocities also indicate the presence of strong solitons and a steep ITB with onshore velocities of 0.10-0.12ms^{-1}, which result in large suspended sediment loads seen in the backscatter profile of Figure 27d. At the maximum amplitude displacement of the soliton during YD 191.16, a significant increase in backscatter is seen as well as during the multiple soliton events on the ITB occurring during YD 191.24-191.26. Unlike during the high wave energy days, where it was shown that surface gravity wave forcing was strong enough to suspend sediment, it is the solitons and the ITB that are generating the friction velocities seen in Figure 27d that lead to sediment suspension. The sharp pulses of the solitons in this case, are seen to only slightly increase values of q' and u_* past the critical values, but are still capable of causing sediment suspension as indicated in the backscatter timeseries.

YD 214.27 in Figure 28 is an example of a low wave energy day coupled with a very broad ITB at the beginning of the 3-hour time period and distinct soltion pulses and a second ITB towards the end of the period. The low wave energy is again evident in the RMS wave velocities of 0.04ms^{-1} in Figure 28a. Despite the low surface gravity wave forcing, the backscatter timeseries indicates that sediment suspension is occurring (Figure 28d). When compared with the CS ADCP and BCDV velocity timeseries, the increases in backscatter occur during the passage of the SIWs and ITBs. The near bed CS velocities of Figure 28b indicate multiple SIWs occuring at YD 214.22 and YD214.34 with strong offshore velocities of 0.07-0.10ms^{-1}. These ITBs are strong enough to generate friction velocities capable of suspending sediment as indicated by the q' and u_* timeseries of Figure 28c and 28d.

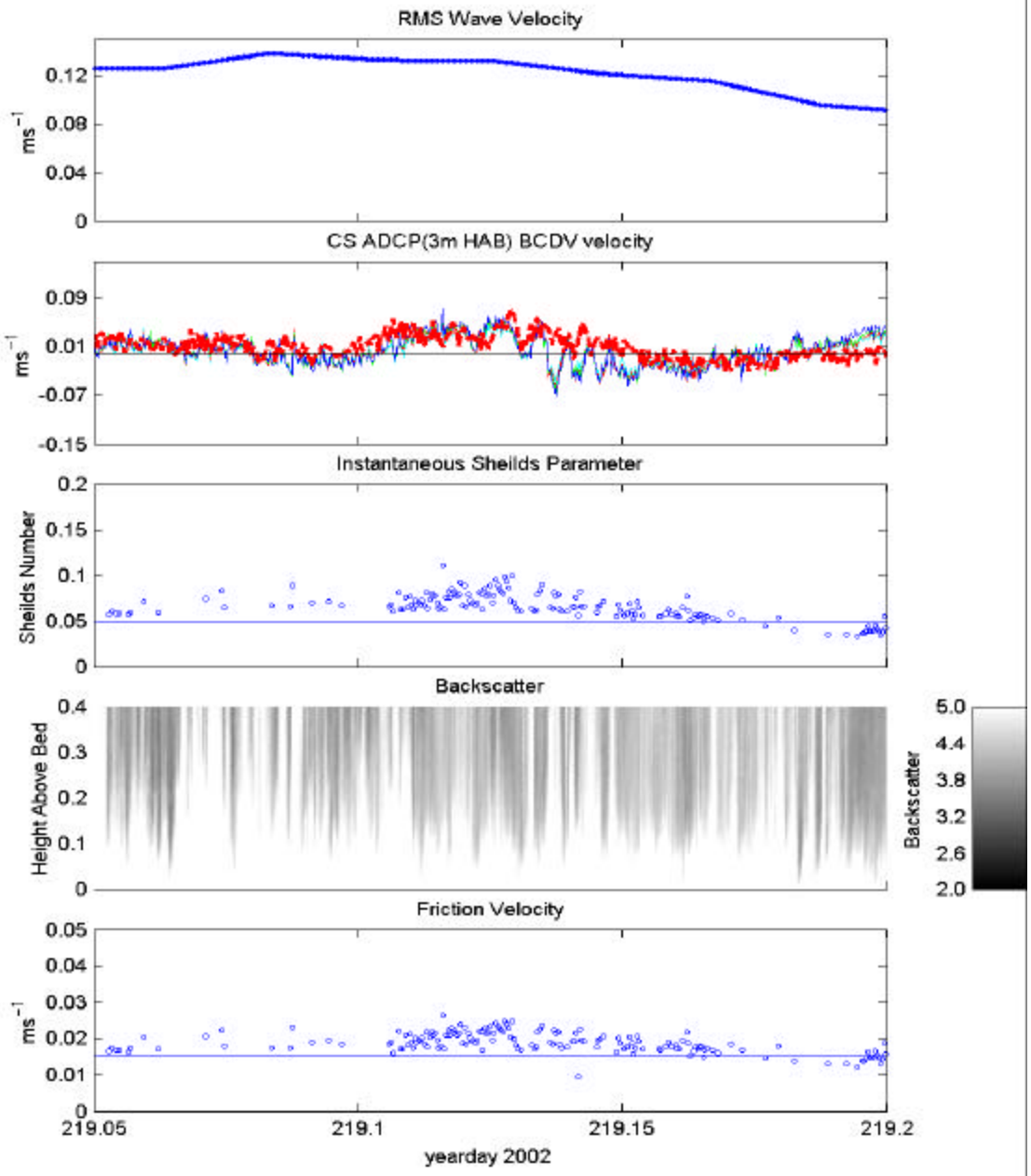

Figure 26. YD 219.05-219.2. (a) RMS Wave Velocity (b) CS ADCP (3m HAB) (bold line) and BCDV (4-18cm HAB) (c) Instantaneous Shields Parameter q_{crit}=0.05 is denoted by the threshold line (d) Backscatter profile timeseries (e) Friction Velocity u* u_{*crit}=1.51cms^{-1} is denoted by the threshold line.

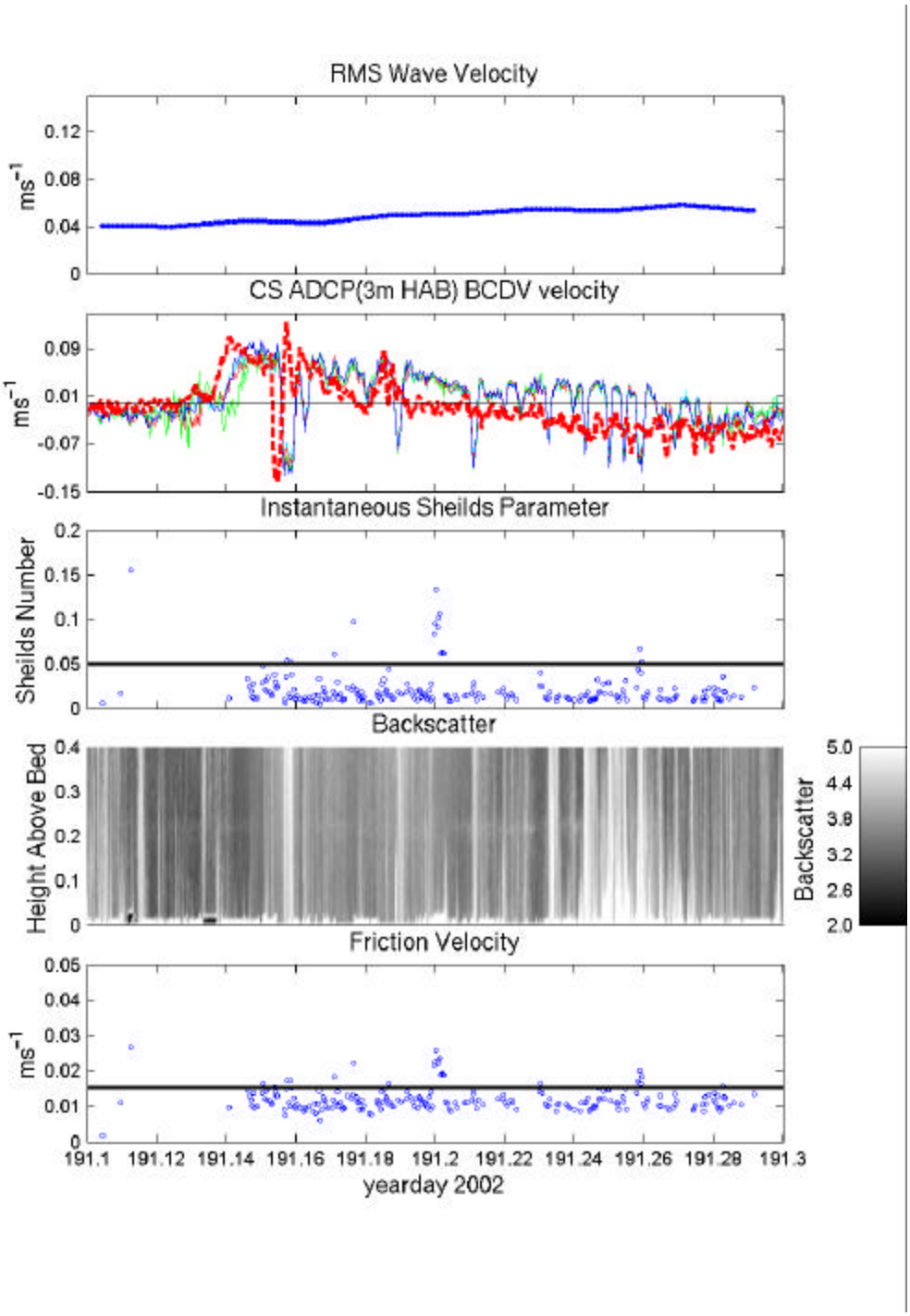

Figure 27. YD 191.1-191.3. (a) RMS Wave Velocity (b) CS ADCP (3m HAB) (bold line) and BCDV (4-18cm HAB) (c) Instantaneous Shields Parameter q_{crit}=0.05 is denoted by the threshold line (d) Backscatter profile timeseries (e) Friction Velocity u* u_{*crit}=1.51cms^{-1} is denoted by the threshold line.

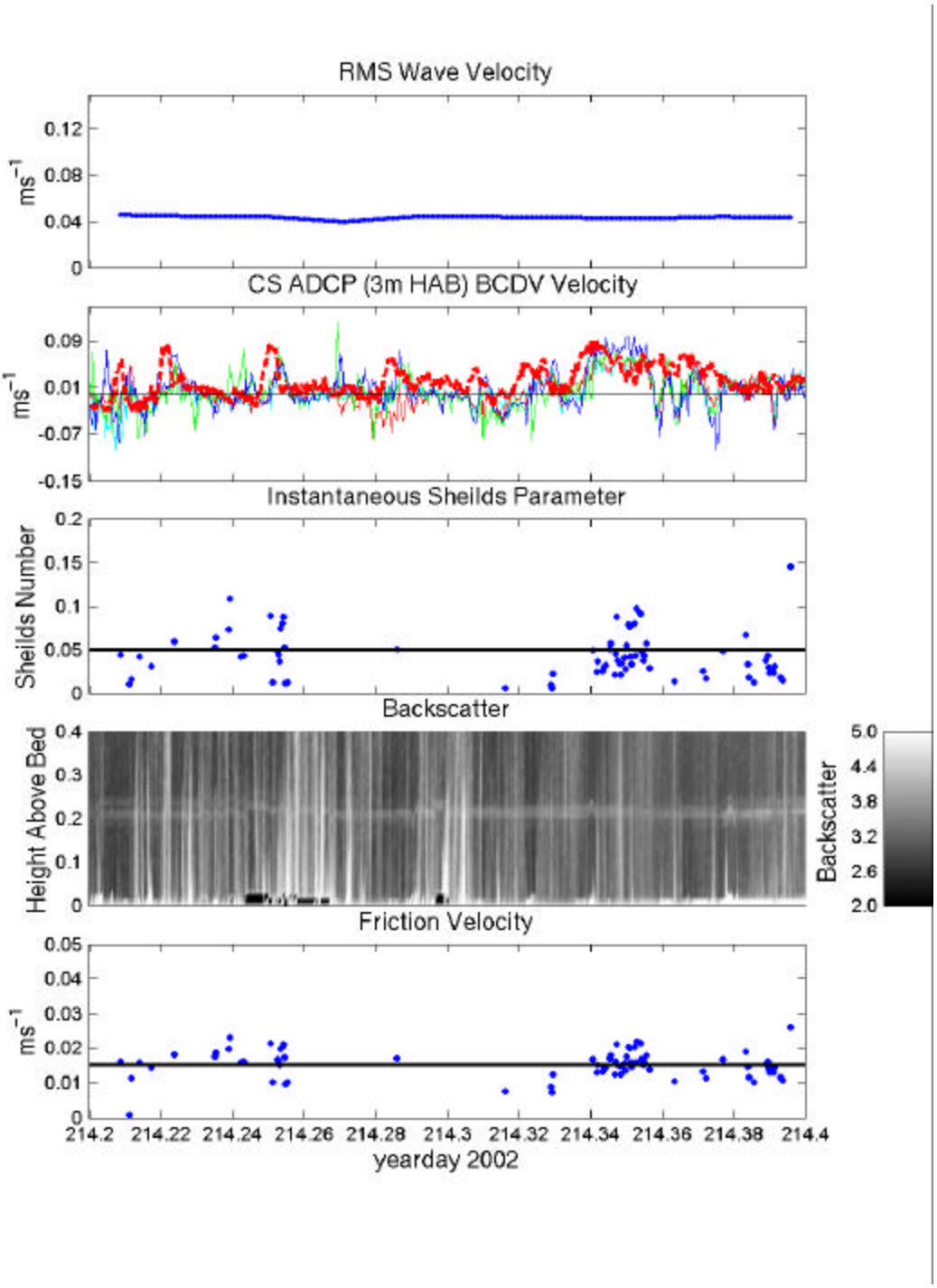

Figure 28. YD 214.2-214.4. (a) RMS Wave Velocity (b) CS ADCP (3m HAB) (bold line) and BCDV (4-18cm HAB) (c) Instantaneous Shields Parameter q_{crit}=0.05 is denoted by the threshold line (d) Backscatter profile timeseries (e) Friction Velocity u* u_{*crit}=1.51cms^{-1} is denoted by the threshold line.

YD 228-228.15 is another low surface gravity wave energy coupled with a single soliton and a steep edged ITB shown in Figure 29. The low wave energy is again evident in the RMS wave velocities of Figure 29a where values are on the order of $0.4 ms^{-1}$. This low surface gravity wave forcing is clearly reflected in the backscatter timeseries of Figure 29d, where shades of black and gray completely dominate the timeseries, indicating no sediment suspension is occurring above the bed. However, light areas 1.5-2 orders greater in magnitude are occurring at approximately YD 228.08. By comparing this to the near bed CS ADCP and BCDV velocities in Figure 28b, it is seen that the single soliton and steep leading edge of the ITB are again the main causes in backscatter increase. These events are generating weaker near bed currents up to $0.04 ms^{-1}$. Timeseries of q' and u_* indicate periods that exceed the critical values, although some of these values appear to be bad data points.

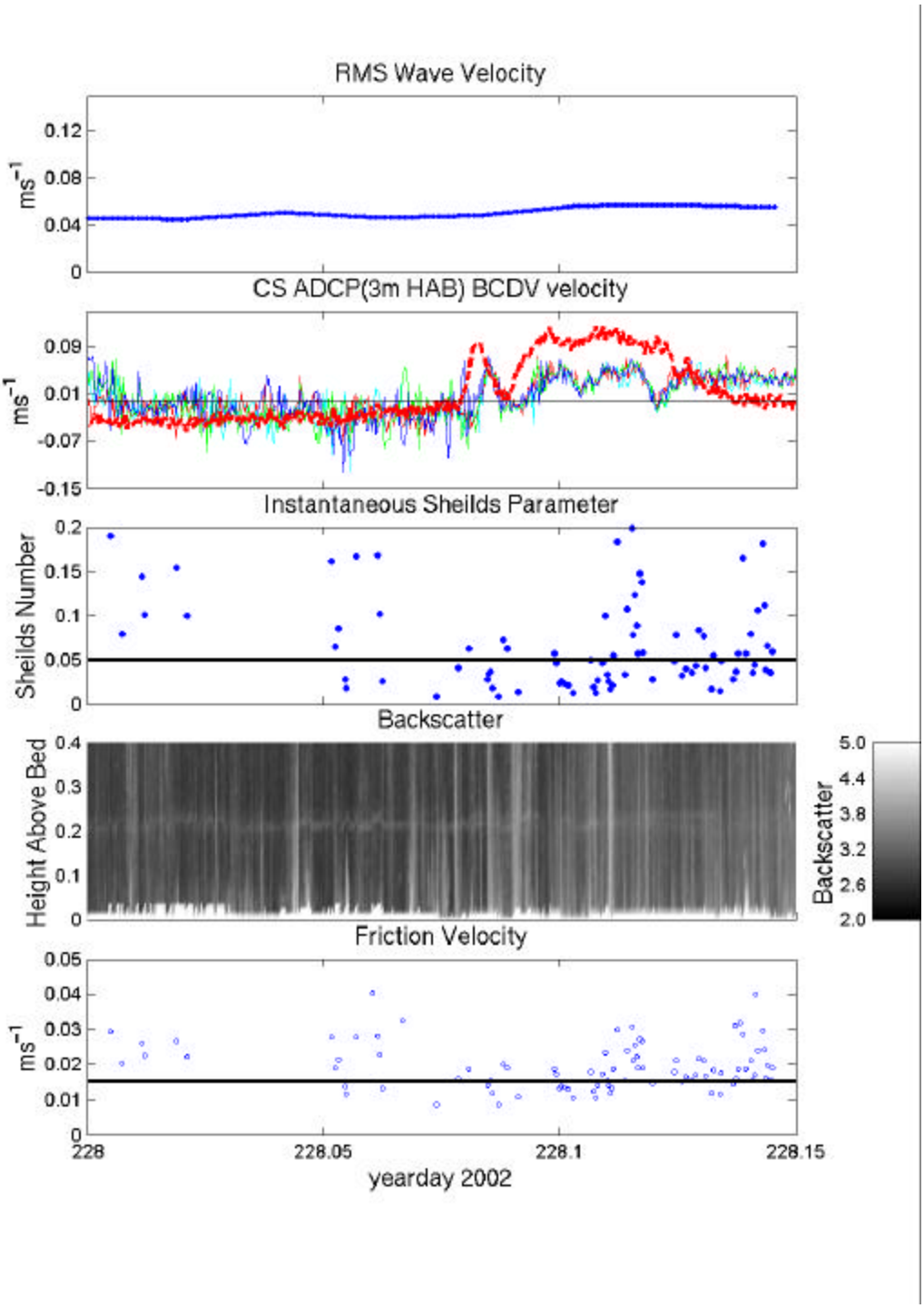

Figure 29. YD 228-228.15. (a) RMS Wave Velocity (b) CS ADCP (3m HAB) (bold line) and BCDV (4-18cm HAB) (c) Instantaneous Shields Parameter q_{crit} = 0.05 is denoted by the threshold line (d) Backscatter profile timeseries (e) Friction Velocity u* u_{*crit}=1.51cms^{-1} is denoted by the threshold line. This is a low wave energy day, which is evident in the backscatter (areas of black/dark gray). Solitons are evident in both the CS BCDV and ADCP and are strong enough to cause sediment suspension (areas of white).

V. DISCUSSION

Solitary internal waves (SIWs) and internal tidal bores (ITBs) acting with surface gravity wave forcing frequently provide the necessary stress above the bed to suspend sediment and organisms that live on the bed into the water column. We hypothesize that the strong, unidirectional flows associated with SIWs and ITBs result in significant net cross-shelf transport of this suspended load in comparison with background currents at this site. This cross-shelf transport of organisms can affect migration, reproduction, and feeding of these and other organisms.

Solitons and ITBs were observed daily during July and August 2002. At least 2 ITBs occurred daily, with one usually being more dominant than the other and moving in either a cross-shore (CS) or alongshore (AS) direction. Multiple solitons were frequently observed on the strong CS bores in contrast to the AS bores that carried with them at most only one dominant soliton. Because these events occurred during most tidal cycles during our observation period, they are potentially responsible for a large part of sediment and biologic entrainment and transport within on the inner shelf within Monterey Bay.

These events consist of strong unidirectional pulses of current, unlike the oscillatory motion of the waves. Therefore, wave forcing will help to suspend and entrain sediment, but solitons and tidal bores provide the dominant forcing for net transport.

A. SEDIMENT SUSPENSION

In the results section, it was shown that solitons and internal tidal bores interacted with the bottom boundary layer through the formation of a logarithmic layer due to skin friction drag along the bed and that the flow over the bed caused by these events can be considered as a wall bounded shear flow. From the slope of this logarithmic layer, the friction velocity was determined and the current stress ($t_{current}$) above the bed can be estimated as

$$t_{current} = r u_*^2 \tag{18}$$

where r is the density of the water and u_* is the friction velocity.

By combining the stress due to the current and the stress due to the surface gravity waves (t_{wave}), the total bed stress (t_{bed}) can be determined.

$$t_{bed} = t_{current} + t_{wave} \tag{19}$$

The stresses from the current and the wave can be broken down into individual components for the current and the wave

$$t_{bed} = t_{SIW} + t_{IT} + t_{LF} + t_{wave} \tag{20}$$

where t_{SIW} is the soliton component, t_{IT} is the internal tidal bore component, and t_{LF} is the low frequency component consisting of wind and tidal forcing. The SIW and IT contributions have been isolated temporarily in this analysis, while t_{LF} is estimated from conditions when ITBs and SIWs are absent.

As stated above, the stress from the current can be directly found through the friction velocity that was derived from the slope of the logarithmic layer by using the Law of the Wall. The stress from the wave can be further broken down to

$$t_{wave} = \frac{1}{2} r f_w (u^2_{waveRMS} + v^2_{waveRMS}) \tag{21}$$

where f_w is the wave friction factor following Jonsson (1967). This is obtained using the median grain size of the sediment (d_{50}) and the RMS wave orbital diameter (a) that can be obtained by integrating the RMS wave velocities ($u^2_{waveRMS} + v^2_{waveRMS}$), measured over a bandwidth from 30Hz to the Nyquist frequency (0.2Hz), with respect to their frequency, giving

$$f_w = \exp[5.213(\frac{2.5d_{50}}{a})^{0.194} - 5.977] \tag{22}$$

Inspection of timeseries in low current, high wave conditions suggests a factor of $2f_w$ better matches critical Shields number criteria, and this has been used in Figures 24-29.

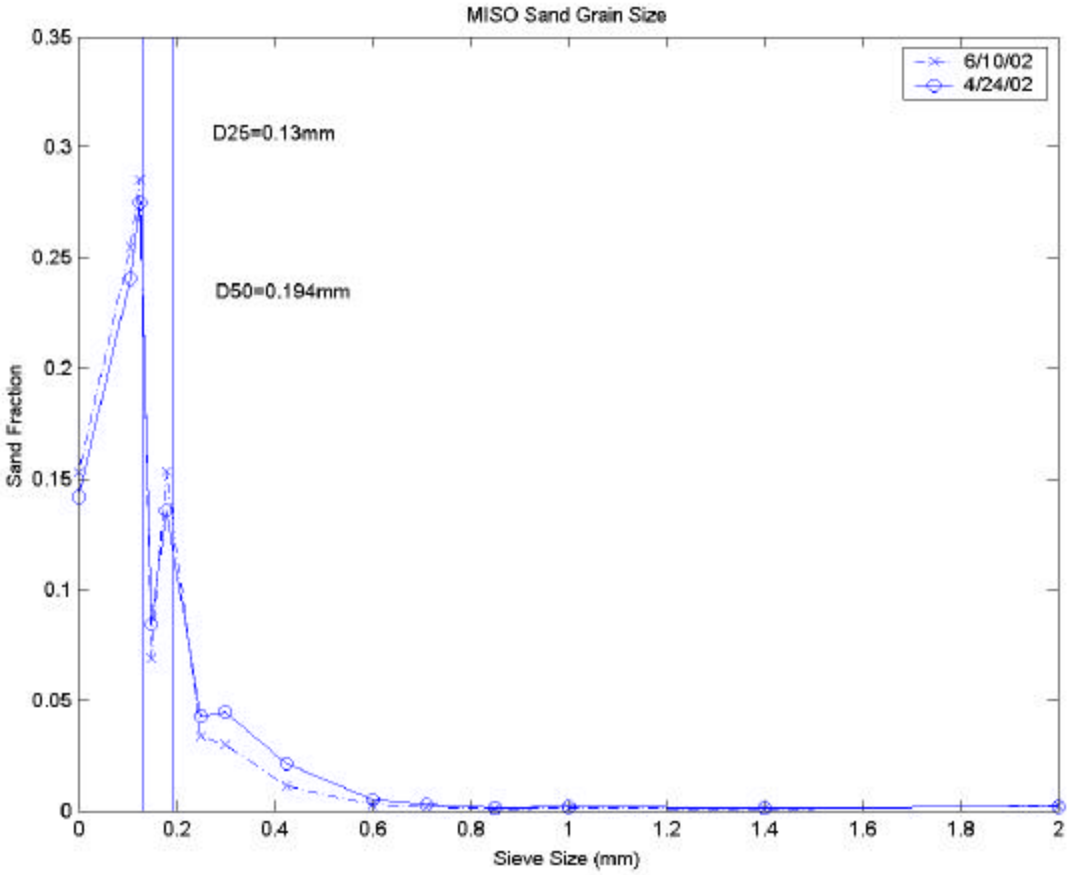

Figure 30. The median grain size (d_{50}) at the MISO site was found to be 0.19mm using in-situ sediment samples taken from April and June 2002. These samples represent a typical log-normal distribution of a single population of well sorted sand in Monterey Bay.

A median grain size (d_{50}) of 0.19mm was measured using in-situ sediment samples taken in April and June 2002 from the MISO site (Figure 30).

Once the total stress felt above the bed was computed, it can be determined whether or not the stress was sufficient enough to lift and suspend sediment. The point at which sediment suspension is initiated occurs when the lifting force due to the stress is strong enough to overcome the gravitational restoring forces on the grain. The Shields Parameter (q') (Shields 1936) states this simple ratio as

$$q' = \frac{t_{current} + t_{wave}}{r(s-1)gd_{50}} \tag{23}$$

where s is the ratio of sediment density to that of water ($\frac{\rho_{sediment}}{\rho_{water}}$) taken to be 2.65 for quartz, g is the gravitational constant at $9.8 ms^2$, and d_{50} is the median grain size found to be 0.19mm. This value represents the instantaneous Shields Number at a given time for the given forcing conditions.

Sediment suspension is initiated when the values for q' exceed a critical Shields number (q_c') of 0.05, which requires a critical friction velocity u_{*_c} of $1.51 cms^{-1}$ for the sediment observed at the MISO site.

In this analysis, the objective is to determine which factors are responsible for sediment suspension near the bed. Solitary internal wave forcing, internal tidal forcing, lower frequency forcing such as winds, as well as wave forcing will all be compared to determine which contributes the most stress that leads to sediment suspension.

1. Wind Forcing

Winds are predominantly from the northwest year round in Monterey Bay except when strong storms move through the region and disrupt the pattern. Figure 30 shows the hourly sampled winds for Monterey Bay as measured by the MISO MET instrument located directly onshore from the MISO site for July and August 2002. These winds have been rotated into a CS normal coordinate system and indicate that winds are predominantly onshore with a positive AS component. Wind forcing should only be felt in the near surface waters since stratification prevents wind driven motion from continuing down through the water column and affecting currents near the bed. By comparing the CS wind components with the CS current components at 10m HAB and 3m HAB, the effects of wind forcing on currents near the surface and near the bed can be determined.

A cross correlation between hourly sampled CS winds and CS currents at both 10m and 3m HAB in Figure 31 shows that there is a higher correlation between wind and current at 10m HAB vice 3m HAB for AS components. CS components at 10m HABhad a negative correlation while at 3m HAB no significant correlation was seen. The AS components at 10m HAB had a positive correlation that was significantly larger than the

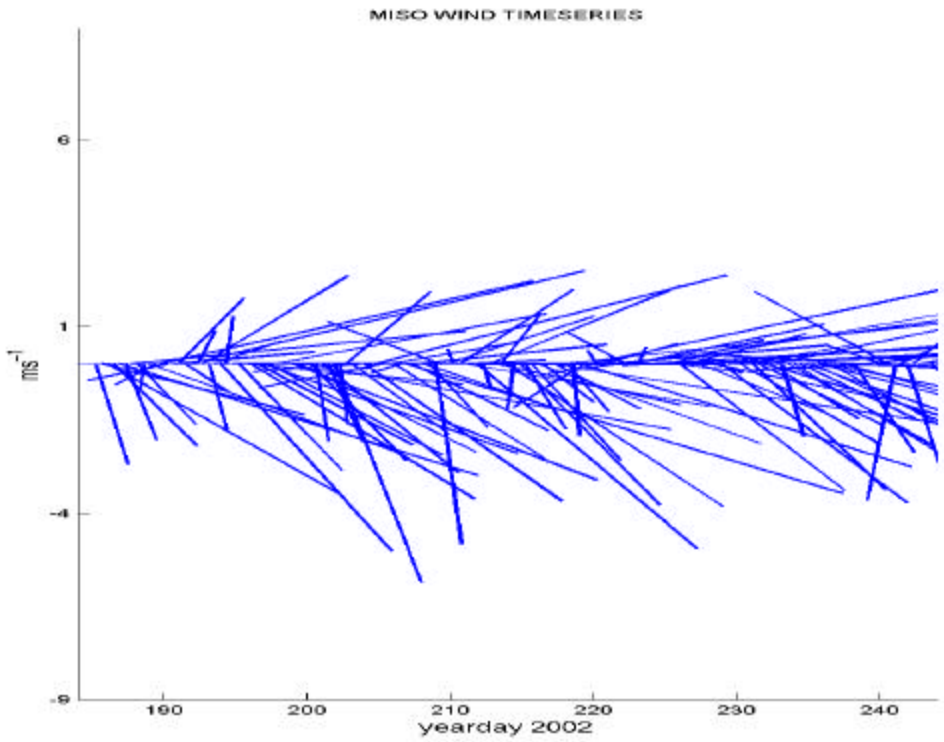

Figure 31. MISO wind timeseries for YD 184-244. Hourly averaged winds show strong diurnal variability and a predominantly northwest duration with a strong onshore component.

correlation at 3m HAB. The low correlations for both AS and CS components indicate that the winds within Monterey Bay have only a slight influence on currents 2m below the surface and almost no influence on currents 10m below the surface for both CS and AS components. This confirms that the stratification present within the water column largely decouples wind driven motion the lower part of the water column, and therefore prevents wind forcing from having any significant effect on the contribution to the stress above the bed.

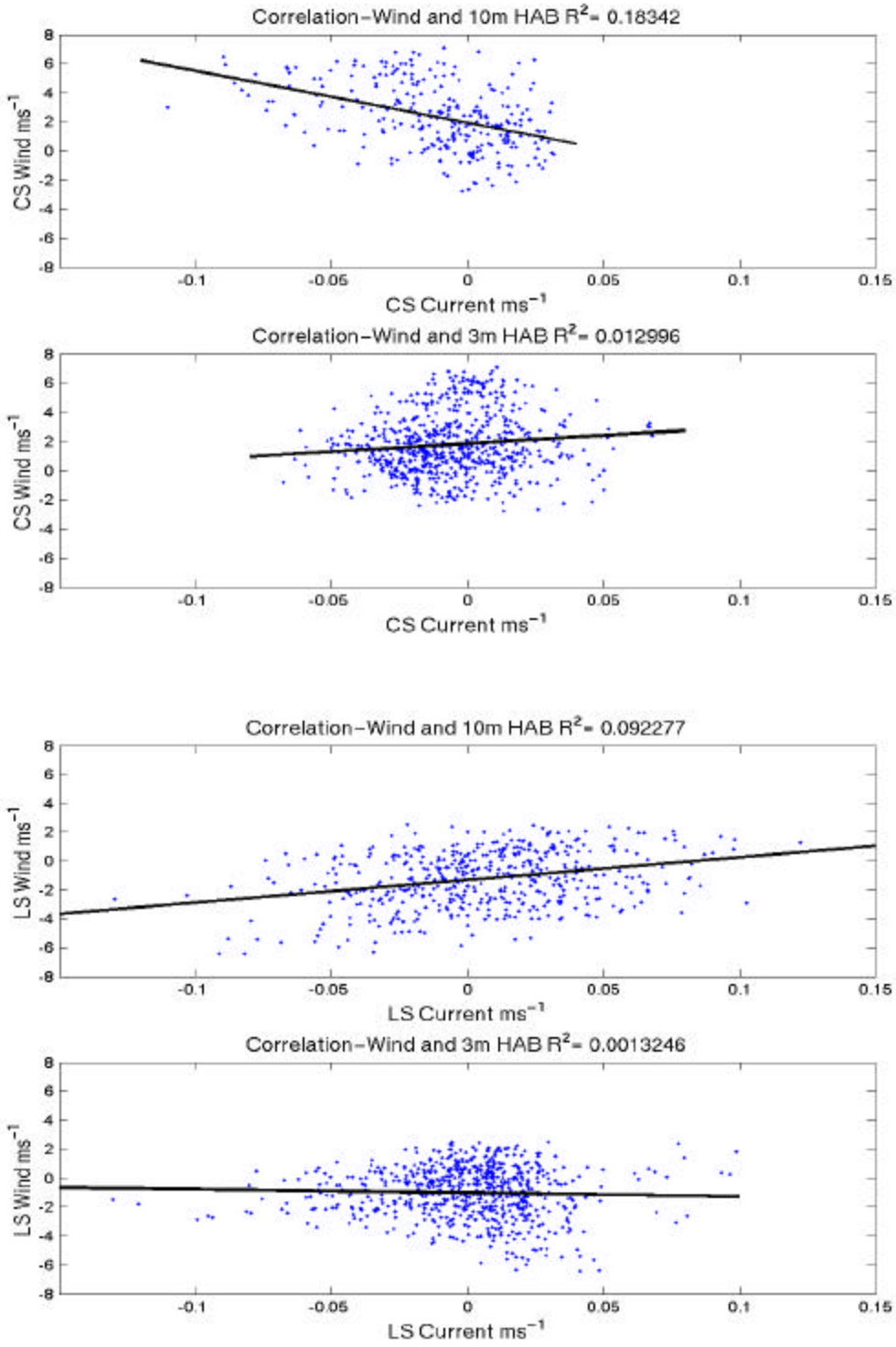

Figure 32. Correlations between wind and current for YD 200-230. (a) AS wind versus AS currents have a higher correlation at 10m HAB vice 3m HAB. (b) CS wind versus CS currents follow the same pattern.

2. Internal Tidal Bores, Solitons, and Wave Forcing

The solitons and internal tidal bores observed during the two month observation period were frequently the dominant currents felt in the bottom 1/3 of the water column, indicating that they most likely disturbed the bed. The resulting current flow over the rough bed generates a logarithmic layer typically extending 20-300cm above the bed, allowing ITB and SIW friction velocity timeseries to be generated (see Figures 24e-29e). With this friction velocity, the corresponding stress above the bed due to the event was calculated as shown by equation 17.

By examining the RMS wave velocities over the same two-month observation period, stress produced by waves can be compared to the stress produced by the solitons and internal tidal bores. From this, it can be determined whether the dominant stress felt above the bed is due to the waves or to the solitons and tidal bores. Figures 24e, 25e, and 26e show the friction velocity timeseries for the three case studies of high wave energy days (YDS 200.8, 206.05, and 219.05). The surface gravity wave velocities as well as the solitons and tidal bores that occurred during each day were strong enough to generate a logarithmic layer above the bed and, therefore, allow a friction velocity to be estimated. RMS velocities due to surface gravity waves ranged from 0.04-0.12 ms^{-1} causing u_* values to exceed the critical friction velocity, indicating that strong wave forcing coupled with a soliton and internal tidal bore event provided enough friction velocity to suspend sediment. Figure 33 summarizes the estimated $u_{*\ \mathrm{wave}}$ and $u_{*\ \mathrm{current}}$ that comprises the SIWs and ITBs. The surface gravity wave energy is shown to have significantly higher values of u_* when compared to u_* values from the baroclinic currents, except for the strong ITB events starting on YD 200.92. However, by combining these two u_* components, the overall u_* greatly exceeds the critical value, so the high suspended load seen in the acoustic backscatter profiles in Figures 24d-26d are expected. For these forcing conditions, surface gravity wave forcing has proved itself to be the dominant factor in contributing to bed stress with the solitons and tidal bores enhancing the stress above the bed.

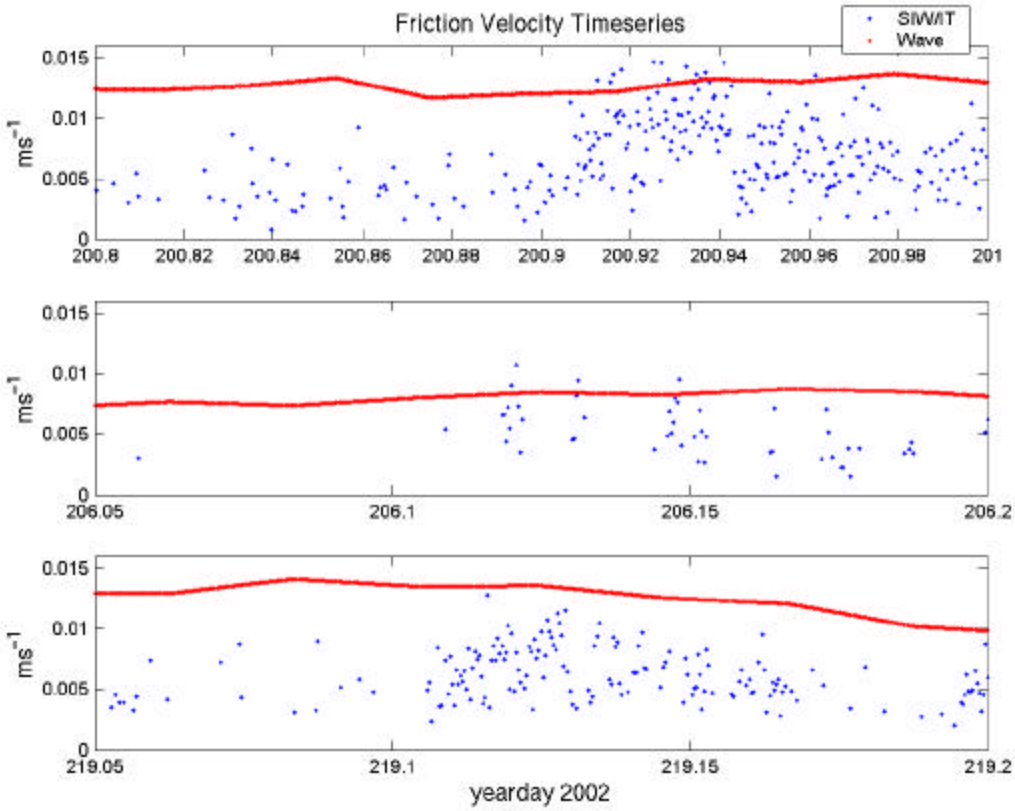

Figure 33. Friction velocity timeseries (u_*) for high wave energy days (YDS 200.8, 206.05, and 219.05). u_* due to the waves is significantly higher than u_* due to the solitons and internal tidal bores. In these cases, surface gravity wave energy is suspending sediment inferred from the acoustic backscatter.

The counter examples of low wave energy days (YDS 191.1, 214.2, and 228) are shown in Figures 25d-28d respectively. In these cases, the surface gravity wave energy was not strong enough to cause sediment suspension by itself, but rather dependent on the additional bed stress due to the solitons and internal tidal bores that occurred during each time period. The total friction velocities generated by the waves and currents were below the critical value of $1.51 cms^{-1}$. Figure 34 shows the friction velocity due to the waves and the currents. Unlike the high wave energy cases where u_{*waves} was significantly higher than $u_{*current}$, the low wave energy days cause u_{*waves} to be on the same order or lower than $u_{*current}$.

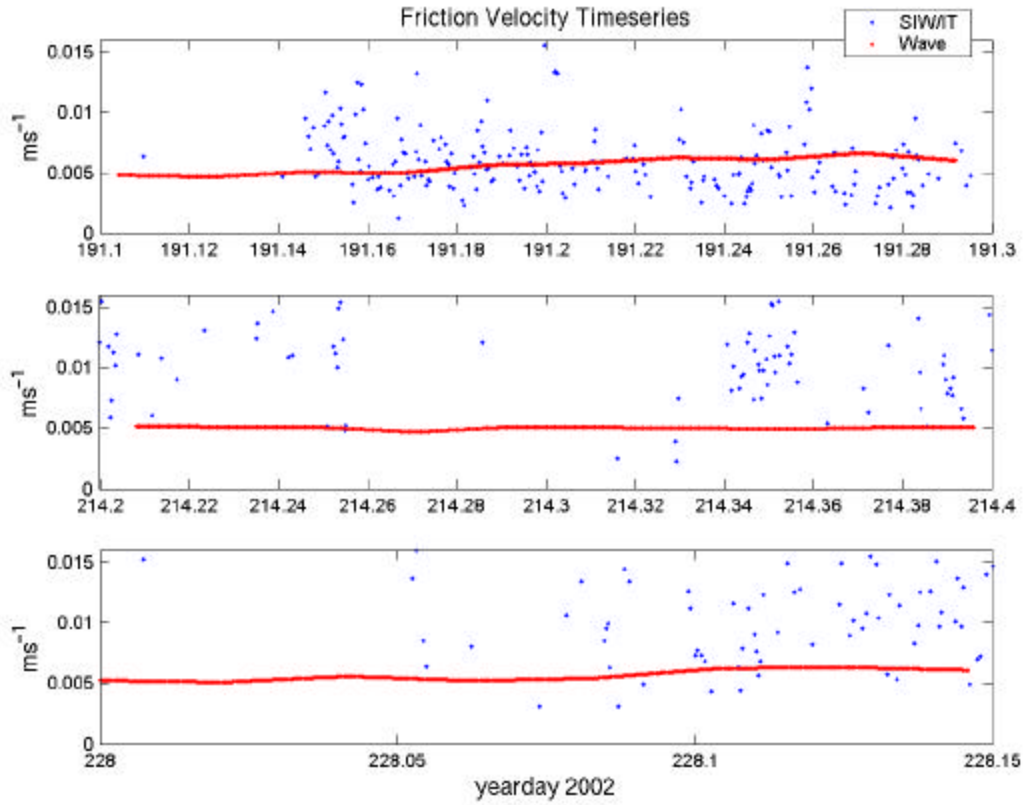

Figure 34. Friction velocity timeseries (u_*) for low wave energy days (YDS 191.1, 214.2, and 228.0). u_* due to the waves is significantly lower than u_* due to the solitons and internal tidal bores. In these cases, surface gravity wave energy is not suspending sediment inferred from the acoustic backscatter.

The different u_* values for high and low surface gravity wave forcing indicates that periods of low wave forcing play no significant role in contributing to bed stress and sediment suspension. The main contribution to bed stress for low surface gravity wave forcing was due primarily to solitons and ITBs. However, strong wave forcing creates a wave boundary layer in the lower portion of the logarithmic layer that decouples the fluid from above and creates more stress above the bed. In a log profile of current velocity versus depth, a sharp bend in the log layer is seen in the lower 1-4 cm (Figure 21) as well as higher velocities up through the layer. When coupled with a soliton or internal tidal bore event, the stress above the bed was seen to increase significantly, resulting in sediment suspension.

B. NET TRANSPORT

Unlike solitons and internal tidal bores which are strong unidirectional pulses of current, oscillatory motion due to surface gravity waves are largely linear and sinusoidal, which over time, averages to no overall net transport. We hypothesize that the net sediment displacement and water column transport at this site is the dominated by currents induced by solitons and ITBs. The net transport of water through the water column was analyzed by integrating 10m and 3m HAB ADCP velocities along with 30cm, 10cm and 3cm HAB BCDV velocities to obtain water column displacement at each level for selected time intervals. The six case studies of high and low wave energy events will be used again to analyze the net transport associated with each event.

For the high wave energy days (YDS 200.8, 206.05, and 219.05) in Figures 24-26 where a strong onshore tidal bore and soltions were observed, net transport in Figure 35 is shown by integrating over the period of the soliton and internal tidal bore at selected HABs. For the YD 200.92 case in Figure 35a, net transport is directed offshore and towards Monterey due to the pulse like current of the soliton and ITB (see timeseries in Figure 24b). However, at 10m HAB, the water has been displaced in an onshore direction as is characteristic with CS bores and solitons. In the YD 206.05 case (see timeseries in Figure 25b), displacement at 10m HAB has a strong AS component in combination with its CS movement resulting in a loop-like motion that is likely the result of a more vortical mode baroclinic bore passing the observation site (Figure 35b). YD 219.05 (see timeseries in Figure 26b) shows quite the opposite results in net transport. In this case, water from 10m down is being displaced in an offshore direction. However, as the bore continues to pass through, water near the bed undergoes several CS oscillations associated with more linear near-bed internal waves (Figure 35c).

The same integration was done for the case studies of low wave energy days. For YD 191.1 (see timeseries in Figure 27b), waters below 3m HAB are being transported offshore during the entire length of the soliton and bore event. At 3m HAB and 10m HAB, there is dominantly onshore transport with a depth dependent AS component (Figure36a). For YD 214.2 (see timeseries in Figure 28b), net transport for levels 3m to 3cm HAB is being directed offshore with a nearly equal −AS component (Figure 36b)

and a less clear baroclinic structure, since transport at all the selected levels is largely in the same direction. YD 228 (see timeseries in Figure 29b) was described as an example of a strong CS propagating bore. This CS movement is seen in the displacement at all levels. Onshore transport is occurring at 10m HAB, while from 3m-3cm HAB, a net offshore transport is occurring within the water column (Figure 36c).

It has been shown that significant wave forcing, along with solitons and ITBs can generate the required friction velocity to overcome the u_{*crit} and provide the necessary stress to initiate sediment motion past the critical Shields Number. Once sediment has been suspended and entrained in different levels above the bed, the strong unidirectional pulses of solitons and tidal bores will cause a significant net transport within the water column. For ITBs generated at the shelf break directly offshore of MISO, net transport is directed largely cross-shelf. However, for those bores generated at the axis of the Monterey Canyon to the north, net transport is directed more AS, but with a more vortical, looped motion for the less steep ITBs.

From these observations, we can conclude that surface gravity wave forcing is significant in suspending sediment during high wave energy days, but rather insignificant for low wave energy days. It was also shown that stronger solitons and tidal bores produced sufficient bed stress to suspend sediment with or without wave forcing. Time integration of velocity profiles show that SIWs and ITBs were largely responsible for the net transport of water and sediment within the water column.

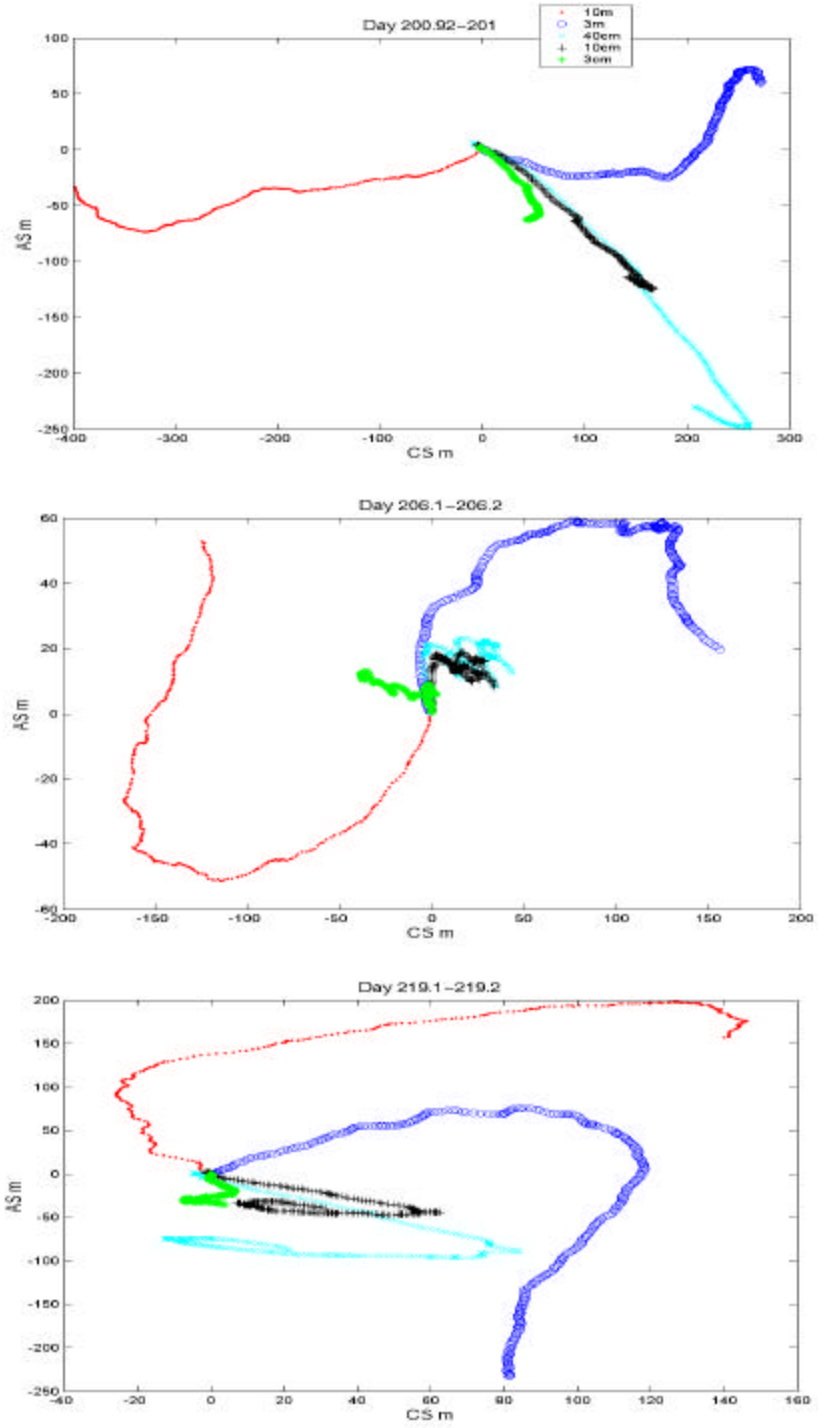

Figure 35. Time integrations for strong tidal bore event and soliton events occurring during YDS 200.8 (a), 206.05 (b), and 219.05 (c) showing net transport at different levels within the water column.

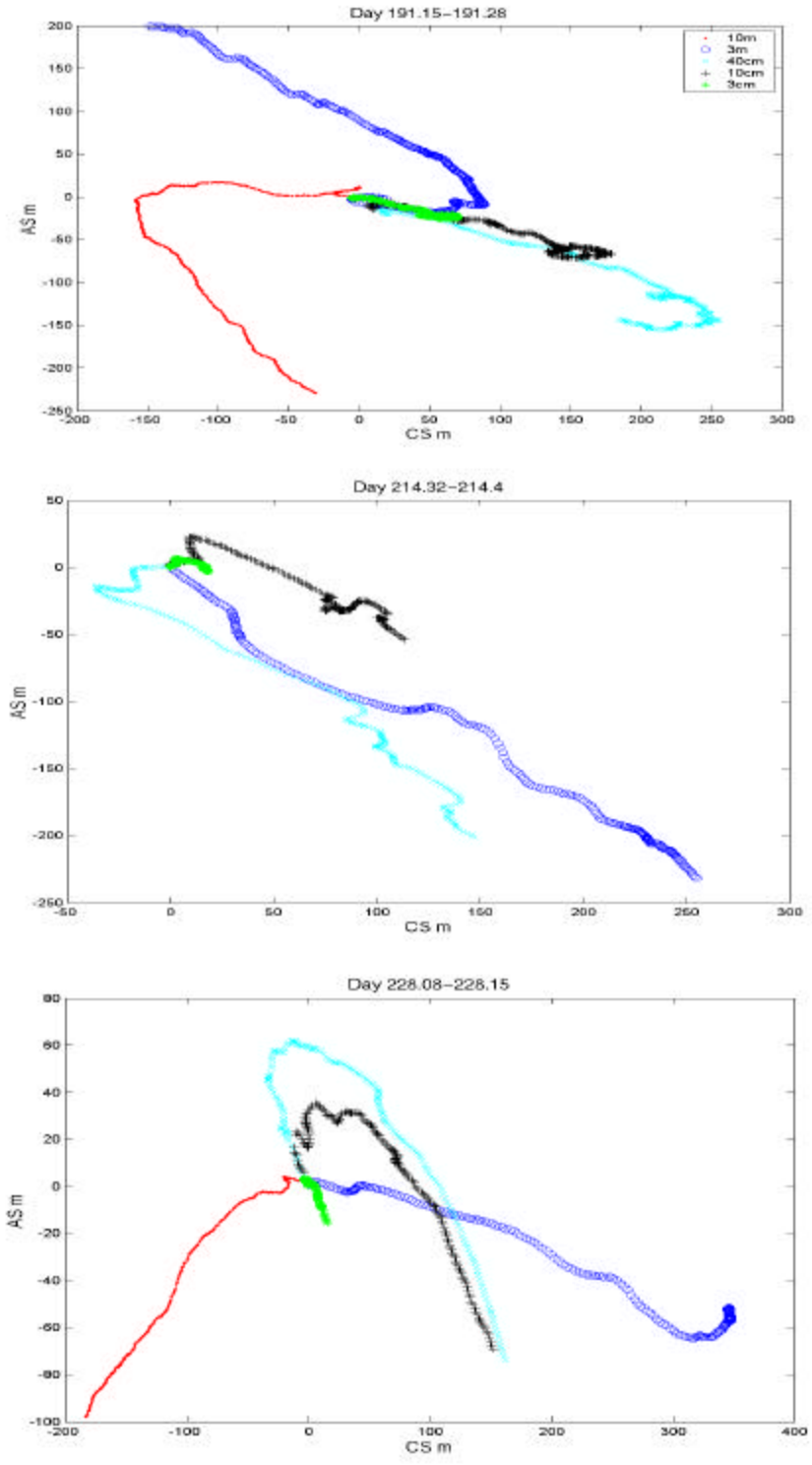

Figure 36. Time integrations for strong tidal bore event and soliton events occurring during YDS 191.1 (a), 214.2 (b), and 228.0 (c) showing net transport at different levels within the water column.

THIS PAGE INTENTIONALLY LEFT BLANK

CONCLUSIONS

Strong internal tidal bores and solitons were observed very close to the nearshore, less than 600 km from the surfzone at the inner shelf MISO site. These highly baroclinic events were evident in both the temperature and velocity profile timeseries in which stratification changed from near surface to near bed and velocities changed from onshore at the surface to offshore near the bed. These events extended down to the bottom 1/3 of the water column as indicated by the velocity and backscatter profile timeseries.

Internal tidal bores were observed daily moving in either a CS or AS direction. The AS bores were most likely generated at the axis of the Monterey Canyon and were refracted to the southern end of the bay. The leading edge of these bores did not degenerate into multiple solitons as their CS counterparts did. The CS bores were generated offshore at the continental shelf break and were not as frequent as the AS bores. However, the leading edges of these bores were able to produce multiple solitons.

Using wall bounded shear flow theory, it has been demonstrated that a logarithmic layer forms due to friction drag as currents flow over the bottom boundary. From this logarithmic layer, the friction velocity and associated stresses were determined for the soliton and tidal bore events and compared with the stresses produced by wave forcing.

The analysis of sediment suspension and transport under the combined forcing of solitary internal waves, internal tidal bores, and surface gravity waves at the MISO site has shown that waves are the dominant force to suspend sediment. However, solitons and internal tidal bores were found to be the dominant force to transport sediment near the bed.

THIS PAGE INTENTIONALLY LEFT BLANK

LIST OF REFERENCES

Apel, J.R. and F.I. Gonzalez, Nonlinear features of internal waves off Baja California as observed from the SEASAT Imaging Radar, *Journal of Geophysical Research*, 88 (C7), 4459-4466, 1983.

Apel, J.R., J.R. Holbrook, J.Tsai, and A.K. Liu, The Sulu Sea internal soliton experiment, *Journal of Physical Oceanography*, 15 (12), 1625-1651, 1985.

Baines, P.G, On internal tide generation models, *Deep-Sea Research*, 29, 3A, 307- 338, 1982.

Baines, P.G., The generation of internal tides by flat-bump topography, *Deep-Sea Research*, 20, 179-205, 1973.

Baines, P.G. and X. Fang, Internal tide generation at continental shelf/slope junction: A comparison between theory and a laboratory experiment, *Dynamics of Atmospheres and Oceans*, 9, 207-314, 1985.

Chapman, R. N. Golenko, V. Paka, K. Sabinin, V. Vlasenko, Generation and Evolution of Internal Waves in the New York Bight during the 1992 JointUS/Russia Internal Wave Remote Sensing Experiment, *Journal of Geophysical Research*, 1997.

Chelton, D. B., A.W. Bratkovich, R.L. Bernseitn and P. M. Korso, Poleward flow off central California during the spring and summer of 1981 and 1984, *Journal of Geophysical Research*, 93, 10,604-10,620, 1988.

Collins, C.A,. Changes in the hydrography of Central California waters associated with the 1997-1998 El Nino, *Progress in Oceanography*, 54,129-147, 2002.

Holloway, P.E., Internal tide generation by seamounts, ridges, and islands, *Journal of Geophysical Research*, 104, C11, 25,937-25,951, 1999.

Holloway, P.E., Internal Hydraulic Jumps and Solitons at a Shelf Break Region on the Australian North West Shelf, *Journal of Geophysical Research*, 92, C5, 5405-5416, 1987.

Jonsson, I.G., Wave boundary layers and friction factors, *Proceedings 10th coastal Engineering Conference*, 1, 127-146, 1966, American Society of Civil Engineers, New York, 1967.

Kropfli, R.A., L.A. Ostrovsky, T.P. Stanton, E.A. Skrta, A. N. Keane, and V.G. Irisov, Relationships between strong internal waves in the coastal zone and their radar and radiometric signatures, *Journal of Geophysical Research*, 1998.

Kundu, P.K., Fluid Mechanics, Academic Press, Inc., 1990.

Liu, A.K., Analysis of Nonlinear Internal Waves in NY Bight, *Journal of Geophysical Research*, 93, C10, 12,317-12,329, 1988..

Paduan, J.D., Wind-driven motions in the Northeast Pacific as measured by Lagrangian drifters, *Journal of Physical Oceanography*, 25,11, 2, 2819-2830, 1995.

Pennington, J.T. and F.P. Chavez, Seasonal fluctuations of temperature, salinity, nitrate, chlorophyll and primary production at station H3/M1 over 1989--1996 in Monterey Bay, California, *Deep Sea Research (Part II, Topical Studies in Oceanography)*, 47, 5-6, 947-973, 1999.

Petruncio E.T., Observations of the Internal Tide in Monterey Canyon, *Journal of Physical Oceanography*, 28, 1873-1903, 1998.

Petruncio E.T., Characterization of tidal currents in Monterey Bay from remote and in-situ measurements. M.S. thesis, Dept. of Oceanography, Naval Postgraduate School, 113pp. [Available from Naval Postgraduate School, Monterey, CA 93943-5000], 1993.

Rosenfeld, L.K., Bifurcated flow from an upwelling center: a cold water source for Monterey Bay, *Continental Shelf Research*, 14, 9, 931-964, 1994.

Shields, I.A., Anwedjung der Aehnlichkeitsmichanic und der Turbulenz-forschung auf die Geschiebebewegung. Mitt. Preuss, Berlin, 1936.

Stanton, T.P., www.oc.nps.navy.mil/~stanton/miso, 1998, January 2003.

Stanton, T.P., and L.A. Ostrovsky, Observation of highly nonlinear internal solitons over the continental shelf, *Geophysical Research Letter*, 25, 14, 1998.

Strub, P.T., J.S. Allen, A. Huyer, R.L. Smith, Seasonal cycles of currents, temperatures, winds, and sea level over the northeast Pacific continental shelf: 35° N to 48° N, *Journal of Geophysical Research*, 92, 1507-1526, 1987.

THIS PAGE INTENTIONALLY LEFT BLANK

INITIAL DISTRIBUTION LIST

1. Defense Technical Information Center
   Ft. Belvoir, Virginia

2. Dudley Knox Library
   Naval Postgraduate School
   Monterey, California

3. Professor Timothy P. Stanton
   Naval Postgraduate School
   Monterey, California

4. Professor Edward B. Thornton
   Naval Postgraduate School
   Monterey, California

5. Professor Mary L. Batteen
   Naval Postgraduate School
   Monterey, California

6. Commander John Joseph
   Naval Postgraduate School
   Monterey, California

7. Professor Curt Collins
   Naval Postgraduate School
   Monterey, California

8. ENS Kristi Tjoa
   Naval Postgraduate School
   Monterey, California